

Differentially Private Normalizing Flows for Density Estimation, Data Synthesis, and Variational Inference with Application to Electronic Health Records

Bingyue Su*, Yu Wang*, Daniele E. Schiavazzi, and Fang Liu

Department of Applied and Computational Mathematics and Statistics,
University of Notre Dame, Notre Dame, IN

Abstract

Electronic health records (EHR) often contain sensitive medical information about individual patients, posing significant limitations to sharing or releasing EHR data for downstream learning and inferential tasks. We use normalizing flows (NF), a family of deep generative models, to estimate the probability density of a dataset with differential privacy (DP) guarantees, from which privacy-preserving synthetic data are generated. We apply the technique to an EHR dataset containing patients with pulmonary hypertension. We assess the learning and inferential utility of the synthetic data by comparing the accuracy in the prediction of the hypertension status and variational posterior distribution of the parameters of a physics-based model. In addition, we use a simulated dataset from a nonlinear model to compare the results from variational inference (VI) based on privacy-preserving synthetic data, and privacy-preserving VI obtained from directly privatizing NFs for VI with DP guarantees given the original non-private dataset. The results suggest that synthetic data generated through differentially private density estimation with NF can yield good utility at a reasonable privacy cost. We also show that VI obtained from differentially private NF based on the free energy bound loss may produce variational approximations with significantly altered correlation structure, and loss formulations based on alternative dissimilarity metrics between two distributions might provide improved results.

keyword: differential privacy, privacy-preserving, synthetic data, normalizing flow, variational inference, free energy bound, KL divergence, density estimation, electronic health records

1 Introduction

1.1 Background

In the last decade, data science has gained tremendous popularity as an interdisciplinary field, thanks to the exponential growth in data volume, fast development of powerful and efficient data analysis techniques, and availability of computational facilities and

*co-first authors

resources. When sharing data among researchers or releasing information to the public, there are always privacy concerns and risks for re-identification or disclosure of sensitive information. Even with key identifiers removed, an adversary may still be able to identify an individual or learn his or her sensitive information, leveraging publicly available data and sophisticated attacks. Some notable privacy attacks includes re-identification based on health records (Sweeney, 1997, 2013), Netflix prize (Narayanan and Shmatikov, 2008), membership attacks (Backes et al., 2016; Homer et al., 2008; Shokri et al., 2017), among others.

In this work, we use electronic health records (EHR) as an example to present approaches for privacy-preserving data sharing and analysis. EHR data often contain sensitive medical information about individual patients. For example, cardiovascular EHRs, the type of EHR data examined in this work, contain measurements of vital signs such as heart rate, arterial and venous, systemic and pulmonary pressures, cardiac output, atrial and ventricular pressures and volumes, ejection fraction, etc., which can be used to diagnose hypertension. Due to privacy concerns, accessing large single-center EHR datasets for research purposes is often problematic (see recent efforts in making large clinical datasets publicly available, for example, the MIMIC-IV dataset discussed in Johnson et al., 2020), not to mention merging multiple EHR data sources to create large multi-center datasets enabling complex predictive models to be trained (see, in this context, the eICU Collaborative Research Database discussed in Pollard et al., 2018).

To mitigate privacy concerns when releasing information and sharing data, various privacy concepts have been proposed over the past two decades, such as k -anonymity (Samarati and Sweeney, 1998), t -closeness (Li et al., 2007), l -diversity (Aggarwal and Yu, 2008), and differential privacy (DP) (Dwork et al., 2006a,b,c), among others. We focus on DP, a popular privacy concept and framework in contemporary privacy research. Besides providing mathematical guarantees on privacy and being robust to various privacy attacks (Dwork et al., 2017), DP has attractive properties, such as privacy loss composition and immunity to post-processing, which have significantly contributed to its popularity for both research and practical applications. Privacy-preserving techniques and algorithms are available for a wide spectrum of statistical and machine-learning methods with DP guarantees, ranging from releasing counts and histograms to predictions from regression models or deep neural networks.

In this work, we examine differentially private normalizing flow (NF) to generate synthetic data via density estimation and to obtain variational inference (VI) with DP guarantees, respectively, under a pre-defined privacy budget. NFs are generative models (Dinh et al., 2016; Kingma et al., 2016; Papamakarios et al., 2017; Rezende and Mohamed, 2015) with major applications in density estimation and VI.

1.2 Our Work and Contributions

Our work comprises two parts. The first part focuses on synthetic data generation from differentially private density estimation and the utility of the synthetic data for downstream learning tasks. To our knowledge, there is only one other paper (Waites and Cummings, 2021) on incorporating DP in NF for density estimation. In addition, no prior work has explored the use of synthetic data generated through DP-NF for downstream learning such as prediction or inference. Our work intends to fill this gap.

Specifically, we apply DP-NF for density estimation given an EHR dataset that contains

hemodynamic measurements from a cohort of patients including individuals suffering from elevated pulmonary pressures (group II pulmonary hypertension, see [Simonneau et al., 2013](#)) and heart failure with preserved ejection fraction ([Harrod et al., 2021](#)). The EHR dataset has a small sample size and a relatively large number of attributes with continuous or discrete numerical measurements and contains missing values. This provides an opportunity to examine the feasibility of DP-NF in generating useful privacy-preserving synthetic data for small-sized datasets, under data type heterogeneity and a greater degree of realism compared to simulated data or well-studied benchmark datasets. We run regression and classification on synthetic data generated by DP-NF and compare their prediction accuracy with that obtained from the original data. We also perform VI of a computationally expensive physics-based model given the synthetic data. To reduce the computation cost, we leverage an offline-trained and fast neural network surrogate model for the physics-based model.

The second part of this work investigates privacy-preserving VI by directly privatizing NF for VI with DP guarantees (as opposed to VI from private synthetic data from differentially private density estimated via NF). We examine the performance of the procedure in inferring the parameters of a nonlinear regression model in simulated data. To the best of our knowledge, this paper is the first to examine the feasibility of differentially privatizing NF for VI using free energy bound loss and stochastic gradient-based optimization. We show that this loss formulation may yield differentially private variational distributions that deviate significantly from the target density, particularly on the correlations if the target distribution is multivariate, when the marginal variances in the differentially private variational distributions are inflated due to DP guarantees compared to the target. We also examined several other dissimilarity metrics as the loss function for NF-VI, similar observations as in the case of free energy bound were observed in some of them, but not all of them. This phenomenon suggests the importance of carefully selecting the loss function when performing VI based on DP-NF.

In both parts, we apply Gaussian DP to achieve privacy guarantees through stochastic gradient descent optimization, in contrast to the moment account method ([Abadi et al., 2016](#)) for tracking privacy loss used in existing work ([Waite and Cummings, 2021](#)). Gaussian DP yields a tighter bound for the privacy loss composition and is shown to yield higher prediction accuracy deep learning (see [Bu et al., 2020](#)), compared to the moment account technique that is based on Rényi DP.

1.3 Related Work

A straightforward approach for differentially private density estimation from which synthetic data can be generated is through histogram sanitization with DP, such as the perturbed histogram or the smoothed histogram approaches ([Wasserman and Zhou, 2010](#)). Histograms as density estimators suffer from the curse of dimensionality, a problem that is only exacerbated after factoring in DP; in addition, continuous attributes need to be discretized in histogram estimators. [Hall et al. \(2013\)](#) and [Alda and Rubinstein \(2017\)](#) develop DP mechanisms to privatize functional outputs with applications to kernel density estimation. Adaptations of local DP to non-parametric density estimation have also been proposed ([Butucea et al., 2020](#); [Kroll, 2021](#)). [Waite and Cummings \(2021\)](#) developed the privacy-preserving version of NF for density estimation by privatizing SGD iteratively with the moment accountant method ([Abadi et al., 2016](#)) to track privacy loss.

Work also exists on VI with privacy guarantees. [Karwa et al. \(2015\)](#) directly model a DP mechanism used for sanitizing a likelihood function and obtain a variational approximation to the resulting sanitized posterior distribution. [Jälkö et al. \(2016\)](#) privatize SGDs using the moment accountant method with an assumed family of variational distributions. [Park et al. \(2016\)](#) develop a privacy-preserving variational Bayes framework by sanitizing the expected sufficient statistics over the distribution of latent variables using the Gaussian mechanism when Bayesian models belong to the conjugate-exponential family. [Sharma et al. \(2019\)](#) examine differentially private VI in the setting of federated learning. [Jälkö et al. \(2022\)](#) propose aligned gradients to factor in the fact that different elements in the gradient vector associated with multi-dimensional variational parameters are often of different magnitudes, aiming to improve the utility of differentially private VI without incurring additional privacy cost. To our knowledge, none of the work above realizes differentially private VI through NF.

Data synthesis for statistical disclosure limitation was first proposed by [Rubin \(1993\)](#) and is employed by government agencies for releasing survey data and by the healthcare industry to share medical data, among other applications. Synthesized surrogate data sets have the same structure as the original dataset but comprise pseudo-individuals. Differentially private data synthesis (DIPS) provides a solution to integrate formal privacy guarantees into data synthesis. DIPS can be achieved through both model-free and model-based approaches; interested readers can refer to [Bowen and Liu \(2020\)](#) for an overview of some of the recent DIPS techniques. The introduction of variational autoencoders (VAE [Kingma and Welling, 2013](#)), generative adversarial networks (GANs [Goodfellow et al., 2014](#)), and NF ([Papamakarios et al., 2017](#); [Rezende and Mohamed, 2015](#)), opened new possibilities for data synthesis through deep-neural-networks-based generative models with DP guarantees. [Xie et al. \(2018\)](#) generate privacy-preserving synthetic data via GANs (DP-GANs), incorporating DP guarantees using the moment accountant method. [Jordon et al. \(2018\)](#) combine GANs and the Private Aggregation of Teacher Ensembles (PATE) framework ([Papernot et al., 2016, 2018](#)) to generate differentially private synthetic data and demonstrate its superiority over DP-GANs in utility in empirical studies. [Chen et al. \(2018\)](#) propose a differentially private autoencoder-based generative model and a differentially private variational autoencoder-based generative model and demonstrate both approaches can yield satisfactory utility but the former is more robust against some privacy attacks than the latter. [Beaulieu-Jones et al. \(2019\)](#) apply DP-GANs to release synthetic data to a real clinical dataset with reasonable DP guarantees and demonstrate the utility of the synthetic data. [Pfitzner and Arnrich \(2022\)](#) generate privacy-preserving synthetic data by aggregating only the decoder component of VAEs in federated learning with DP while leaving the encoders personal at local servers.

The rest of the paper is organized as follows. Section 2 introduces the definitions of NF for density estimation and VI and the concept of DP. Section 3 presents the procedure for differentially private NF for density estimation and generation of privacy-preserving synthesis from estimated density, with an application to a real EHR dataset. Section 4 presents the procedure for differentially private NF for VI, with an application to repeated measures data simulated from a nonlinear model and an in-depth analysis of the utility of variational distributions obtained from the procedure. The paper concludes in Section 5 with a summary and some final remarks.

2 Preliminaries

2.1 Normalizing Flow

Normalizing Flow (NF) is defined as a map $F : \mathbb{R}^d \times \Lambda \rightarrow \mathbb{R}^d$ parameterized by $\lambda \in \Lambda$ transforming realizations from an easy-to-sample base distribution such as $\mathbf{z}_0 \sim \mathcal{N}(\mathbf{0}, I_d)$, to realizations from a desired target density. Specifically, F consists of a composition of K bijections $F_k : \mathbb{R}^d \times \Lambda_k \rightarrow \mathbb{R}^d$, each parameterized by $\lambda_k \in \Lambda_k$: $F_\lambda(\mathbf{z}_0) = F(\mathbf{z}_0; \lambda) = [F_K(\cdot; \lambda_K) \circ F_{K-1}(\cdot; \lambda_{K-1}) \circ \dots \circ F_1(\cdot; \lambda_1)](\mathbf{z}_0)$, where $\mathbf{z}_k = F_k(\mathbf{z}_{k-1}; \lambda_k)$ for $k = 1, \dots, K$. Since $F_k(\cdot; \lambda_k)$ is a bijection from \mathbf{z}_{k-1} to \mathbf{z}_k , $q_k(\mathbf{z}_k)$, the distribution of \mathbf{z}_k , can be obtained by the change of variable

$$q_k(\mathbf{z}_k) = q_{k-1}(\mathbf{z}_{k-1}) \left| \det \frac{\partial F_k^{-1}}{\partial \mathbf{z}_{k-1}} \right| = q_{k-1}(\mathbf{z}_{k-1}) \left| \det \frac{\partial F_k}{\partial \mathbf{z}_{k-1}} \right|^{-1}. \quad (1)$$

Taking the logarithm and summing over k , Eqn. (1) becomes

$$\log q_K(\mathbf{z}_K) = \log q_0(\mathbf{z}_0) - \sum_{k=1}^K \log \left| \det \frac{\partial F_k}{\partial \mathbf{z}_{k-1}} \right|. \quad (2)$$

Generally, the objective of training a NF is to determine an *optimal* set of parameters λ so that q_K can approximate either a target density p (VI) or the distribution of the observed data \mathbf{x} (density estimation).

For general bijections, the computational cost of computing the Jacobian determinants in Eqn. (1) may increase significantly with the dimensionality d and the number of layers K . To efficiently compute these determinants, various NF formulations have been proposed based on coupling layers such as RealNVP (Dinh et al., 2016) and GLOW (Kingma and Dhariwal, 2018), and autoregressive transformations such as MAF (Papamakarios et al., 2017) and IAF (Kingma et al., 2016), both of which are associated with tractable triangular Jacobian matrices and easy to compute.

In the applications of NF to density estimation and VI in Sections 3 and 4, we use MAF (Papamakarios et al., 2017). The autoregressive property of MAF is obtained by setting $p(z_i | z_1, \dots, z_{i-1}) = \phi((z_i - \mu_i)/e^{\alpha_i})$, where ϕ is the density function of the standard normal distribution, $\mu_i = f_{\mu_i}(z_1, \dots, z_{i-1})$, $\alpha_i = f_{\alpha_i}(z_1, \dots, z_{i-1})$, and f_{μ_i} and f_{α_i} are masked autoencoder neural networks (MADE, Germain et al., 2015). Consider \mathbf{z} and $\hat{\mathbf{z}}$ as the input and output of a MADE network having L hidden layers with d_l , $l = 1, \dots, L$ neurons per layer. The mappings between layers could be represented as

$$\begin{cases} \mathbf{y}_1 = h_1(b_1 + (\mathbf{W}^1 \odot \mathbf{M}^1)\mathbf{z}), & \text{where } \mathbf{M}^1 \text{ is } d_1 \times d \text{ and } \mathbf{M}_{u,v}^1 = \mathbb{1}_{m^1(u) \geq v} \\ \mathbf{y}_l = h_l(b_l + (\mathbf{W}^l \odot \mathbf{M}^l)\mathbf{y}_{l-1}), & \text{where } \mathbf{M}^l \text{ is } d_l \times d_{l-1} \text{ and } \mathbf{M}_{u,v}^l = \mathbb{1}_{m^l(u) \geq m^{l-1}(v)} \\ \hat{\mathbf{z}} = h_{L+1}(b_{L+1} + (\mathbf{W}^{L+1} \odot \mathbf{M}^{L+1})\mathbf{y}_L) & \text{where } \mathbf{M}^{L+1} \text{ is } d \times d_L \text{ and } \mathbf{M}_{u,v}^{L+1} = \mathbb{1}_{u > m^L(v)}, \end{cases}$$

where h_l is the activation function between layer $l-1$ and l for $l = 1, \dots, L+1$, $m^l(k)$ is a pre-set or random integers from 1 to $d-1$, b_l and \mathbf{W}^l are the bias and weight parameters for layer $l = 1, \dots, L+1$.

The matrix product $\prod_{l=L+1}^1 \mathbf{M}^l$ is strictly lower triangular, satisfying the autoregressive property (Germain et al., 2015). The masks $\mathbf{M}^1, \dots, \mathbf{M}^{L+1}$ enable the computation of all μ_i and α_i in a single forward pass (Papamakarios et al., 2017). Additionally, the Jacobian of each MAF layer is lower-triangular, with determinant equal to

$|\det \partial f / \partial \mathbf{z}|^{-1} = \exp(\sum_{i=1}^d \alpha_i)$. Before each MADE layer, batch normalization (Ioffe and Szegedy, 2015) can be used to normalize the outputs from the previous layer. Batch normalization performs elementwise scaling and shifting operations, is easily invertible, has a tractable Jacobian, and is found to help stabilize and accelerate training and increase accuracy (Papamakarios et al., 2017).

When NF is employed for density estimation given observed data \mathbf{x} , the following log-likelihood is maximized, assuming n independent observations \mathbf{x}_i , $i = 1, \dots, n$.

$$\begin{aligned} \ell(\lambda; \mathbf{x}) &= \log q_K(\mathbf{x}) = \sum_{i=1}^n \log q_K(\mathbf{x}_i) \\ &= \sum_{i=1}^n \log q_0(\mathbf{z}_{i,0}) - \sum_{i=1}^n \sum_{k=1}^K \left| \det \frac{\partial F_k}{\partial \mathbf{z}_{i,k-1}} \right|, \end{aligned} \quad (3)$$

where $\mathbf{z}_{i,k-1} = F_k^{-1} \circ \dots \circ F_{K-1}^{-1} \circ F_K^{-1}(\mathbf{x}_i)$. Once the NF parameters are obtained via the maximum likelihood approach, samples from q_K can be generated by first sampling from the base distribution and then transforming the samples through a sequence of bijections. NF has been shown to provide accurate approximations of complex density functions of various data types (Dinh et al., 2016; Kingma and Dhariwal, 2018; Papamakarios et al., 2017).

The other major application of NF is VI. Consider the likelihood $l(\mathbf{z}; \mathbf{x})$ of parameters or latent variables \mathbf{z} given observed data \mathbf{x}_i for $i = 1, \dots, n$. Given prior $p(\mathbf{z})$, an NF-based approximation $q_K(\mathbf{z})$ of the posterior distribution $p(\mathbf{z}|\mathbf{x})$ can be computed by maximizing the lower bound to the log marginal likelihood $\log p(\mathbf{x})$ (the *evidence lower bound* or ELBO), or, equivalently, by minimizing the free energy bound (Rezende and Mohamed, 2015), expressed as

$$\begin{aligned} \mathcal{F}(\mathbf{x}) &= \mathbb{E}_{q_K(\mathbf{z})} [\log q_K(\mathbf{z}) - \log p(\mathbf{x}, \mathbf{z})] = \mathbb{E}_{q_K(\mathbf{z}_K)} [\log q_K(\mathbf{z}_K) - \log p(\mathbf{x}, \mathbf{z}_K)] \\ &= \mathbb{E}_{q_0(\mathbf{z}_0)} [\log q_0(\mathbf{z}_0)] - \mathbb{E}_{q_0(\mathbf{z}_0)} [\log p(\mathbf{x}, \mathbf{z}_K)] - \mathbb{E}_{q_0(\mathbf{z}_0)} \left[\sum_{k=1}^K \log \left| \det \frac{\partial F_k}{\partial \mathbf{z}_{k-1}} \right| \right] \\ &= \sum_{i=1}^n \left(\frac{1}{n} \mathbb{E}_{q_0(\mathbf{z}_0)} [\log q_0(\mathbf{z}_0)] - \mathbb{E}_{q_0(\mathbf{z}_0)} [\log p(\mathbf{x}_i, \mathbf{z}_K)] - \frac{1}{n} \mathbb{E}_{q_0(\mathbf{z}_0)} \left[\sum_{k=1}^K \log \left| \det \frac{\partial F_k}{\partial \mathbf{z}_{k-1}} \right| \right] \right) \\ &= \sum_{i=1}^n l_i \end{aligned} \quad (4)$$

The expectations in Eqn. (4) can be approximated by their corresponding Monte Carlo (MC) estimates using samples $\mathbf{z}_{i,0}$, $i = 1, \dots, n$ from the basic distribution q_0 during implementation.

2.2 Differential Privacy

Differential Privacy (DP) is a mathematical framework designed to produce robust privacy guarantees. It aims at protecting privacy of every individual in a dataset in the worst-case scenario.

Definition 1 ((ϵ, δ) -DP). (Dwork et al., 2006a,b,c) A randomized mechanism \mathcal{M} is ϵ -DP, if $\Pr[\mathcal{M}(D_1) \in S] \leq e^\epsilon \Pr[\mathcal{M}(D_2) \in S] + \delta$ for any $S \in \text{range}(\mathcal{M})$ and neighbouring datasets D_1, D_2 that differ by one record, where $\epsilon > 0$ and $\delta \in [0, 1)$.

Informally, DP implies that the chance of identifying an individual in a dataset using a randomized mechanism is limited if the released information is about the same with or

without that individual in the data. The quantities ϵ and δ represent privacy budget or privacy loss parameters. When $\delta = 0$, (ϵ, δ) -DP in Definition 1 reduces to pure ϵ -DP. The smaller the ϵ , the higher the privacy protection there is for the individuals in the data.

When we apply DP mechanisms repeatedly to query a dataset, privacy loss will accumulate during the process. It is therefore necessary to track and account for the accumulated loss so that the privacy loss would not be too large. This has motivated the development of variants and extensions of the original DP concepts, aiming at achieving tighter bounds for composite privacy loss, such as the concentrated DP (Bun and Steinke, 2016; Bun et al., 2018; Dwork and Rothblum, 2016), Rényi DP (Mironov, 2017), and Gaussian DP (Dong et al., 2019). Abadi et al. (2016) propose a widely popular moment account technique based on Rényi DP to track privacy loss in stochastic gradient descent-based optimization. Dong et al. (2019) provide a tighter bound based on Gaussian DP (GDP), which is the DP paradigm we will use for the reminder of this paper.

Definition 2 (μ -GDP). (Dong et al., 2019) Let T be a trade-off function that maps $[0, 1]$ to $[0, 1]$, defined as $T(P_0, P_1)(\alpha) = \inf\{\beta_\phi : \alpha_\phi \leq \alpha\}$ for two distributions P_1 from P_0 to be distinguished through hypothesis testing ($H_0 : P_0$ vs. $H_1 : P_1$), where $\phi \in [0, 1]$ is a rejection rule with the type I error $\alpha_\phi = \mathbb{E}_{P_0}[\phi]$ and type II error $\beta_\phi = 1 - \mathbb{E}_{P_1}[\phi]$. A randomized mechanism \mathcal{M} is of μ -GDP if

$$T(\mathcal{M}(D_1), \mathcal{M}(D_2)) \geq T(\mathcal{N}(0, 1), \mathcal{N}(\mu, 1))$$

for any neighboring datasets D_1, D_2 differing by one record,

The Gaussian mechanism can be applied to achieve μ -GDP guarantees when releasing a statistic or a query result from a dataset.

Definition 3 (Gaussian Mechanism of μ -GDP). (Dong et al., 2019) For a given query f and a dataset D , a Gaussian mechanism $\mathcal{M}(D)$ satisfying μ -GDP is defined as

$$f_{\mathcal{M}}^*(D) \sim \mathcal{N}(f(D), \Delta_f^2/\mu^2),$$

where $\Delta_f = \max_{D_1, D_2} \|f(D_1) - f(D_2)\|_1$ for any pair of neighboring datasets (D_1, D_2) .

Dong et al. (2019) also presents a noisy stochastic gradient descent (SGD) algorithm as a composition of repeated Gaussian mechanisms application with sub-sampling in. If we denote the number of iterations of the SGD algorithm by T , the sub-sampling rate by r , and the scale of noise added to the gradient at each iteration by σ , then the total privacy loss under GDP over T iterations is $\mu = r\sqrt{T(e^{1/\sigma^2} - 1)}$.

There is a duality between (ϵ, δ) -DP and μ -GDP (Dong et al., 2019), which helps to translate the privacy loss between the two DP frameworks. If a mechanism is of μ -GDP, then it also satisfies $(\epsilon, \delta(\epsilon))$ -DP, where $\delta(\epsilon) = \Phi(-\frac{\epsilon}{\mu} + \frac{\mu}{2}) - e^\epsilon \Phi(-\frac{\epsilon}{\mu} - \frac{\mu}{2})$, where Φ is the CDF of the standard normal distribution.

3 Private-preserving Density Estimation and Synthetic Data Generation through DP-NF

In this section, we present differentially private density estimation via NF, which can be used to synthesize privacy-preserving surrogate datasets before their public release.

Users can then conduct statistical analysis or train machine learning algorithms on the synthetic data in the same way as if they had the original data. In what follows, we first present the EHR data that motivates the work, then provide an algorithm to incorporate DP in NF for density estimation, apply the algorithm to generate private EHR data, and finally examine the utility of the surrogate data via downstream learning tasks including classification, regression, and VI.

3.1 Description of the EHR Dataset

The EHR dataset contains anonymized clinical measurements from 82 adult patients. The data were collected in the context of a research project funded by Google through its ATAP initiative, focusing on modeling noninvasive measurements of cardiovascular dynamics. Table 1 lists the 26 clinical attributes present in the dataset with the summary statistics. Figure 1 shows the missing data pattern. Each row of the heat map was normalized to a zero to one range, to highlight the relative magnitude of each clinical target. Each patient has zero to nineteen clinical attributes. While there is not a single patient that has all 26 measurements, at least three clinical attributes (heart rate, diastolic blood pressure, and systolic blood pressure) are available for all but one patient.

Table 1: Summary Statistics on the EHR dataset containing 26 clinical measurements.

	Attribute	Description	Unit	SD*	n [#]	Min	Max
1	heart_rate2	Heart rate	bpm	3.0	81	69.0	105.0
2	systolic_bp_2	Systolic blood pressure	mmHg	1.5	81	83.0	180.0
3	diastolic_bp_2	Diastolic blood pressure	mmHg	1.5	81	49.0	102.0
4	cardiac_output	Cardiac output	L/min	0.2	65	3.3	10.9
5	systemic_vascular_resistan	Systemic vascular resistance	dynes·s·cm ⁻⁵	50.0	64	668.6	2046.8
6	pulmonary_vascular_resista	Pulmonary vascular resistance	dynes·s·cm ⁻⁵	5.0	50	5.0	245.8
7	cvp	Central venous pressure	mmHg	0.5	30	2.0	28.0
8	right_ventricle_diastole	Right ventricle diastolic pressure	mmHg	1.0	11	2.0	10.0
9	right_ventricle_systole	Right ventricle systolic pressure	mmHg	1.0	46	12.0	45.0
10	rvedp	Right ventricle EDP	mmHg	1.0	46	1.0	20.0
11	aov_mean_pg	Average PG across aortic valve	mmHg	0.5	2	5.0	10.0
12	aov_peak_pg	Peak PG across aortic valve	mmHg	0.5	37	3.0	18.0
13	mv_decel.time	Mitral valve deceleration time	ms	6.0	41	88.0	289.0
14	mv_e_a_ratio	Mitral valve E/A ratio	-	0.2	39	0.7	20.9
15	pv_at	Pulmonary valve acceleration time	ms	6.0	18	53.0	190.0
16	pv_max_pg	Peak PG across pulmonary valve	mmHg	0.5	31	1.0	18.0
17	ra_pressure	Mean right atrial pressure	mmHg	0.5	50	3.0	15.0
18	ra_vol_a4c	Right atrial volume	mL	3.0	4	57.0	173.0
19	la_vol_a4c	Left atrial volume	mL	3.0	7	69.0	179.0
20	lv_esv	Left ventricular end-systolic volume	mL	10.0	1	32.0	32.0
21	lv_vol_a4c	Left ventricular volume	mL	20.0	5	59.0	642.0
22	lvef	Left ventricular ejection fraction	-	2.0	53	12.5	75.0
23	lvot_max_flow	Peak flow velocity across LVOT	cm/s	-	0	-	-
24	pap_diastolic	Diastolic PAP	mmHg	1.0	65	5.0	36.0
25	pap_systolic	Systolic PAP	mmHg	1.0	65	10.0	60.0
26	wedge_pressure	Pulmonary wedge pressure	mmHg	1.0	50	2.0	26.0

*standard deviation; determined based on a preliminary literature review (Gordon et al., 1983; Maceira et al., 2006; Yared et al., 2011).

[#]Number of patients with observed measurements on the respective attribute.

This dataset focuses on cases of group II pulmonary hypertension (i.e., hypertensive/not hypertensive), where a reversible increase of PVR follows an increase in left ventricular filling pressures¹. A often used binary classification in practice is a criterion based on

¹We do not consider pulmonary arterial hypertension (group I pulmonary hypertension) nor make any claim of differentiating group I and II pulmonary hypertension. Other criteria have been proposed to classify hypertension due to left ventricular diastolic dysfunction (see, e.g., Simonneau et al., 2013).

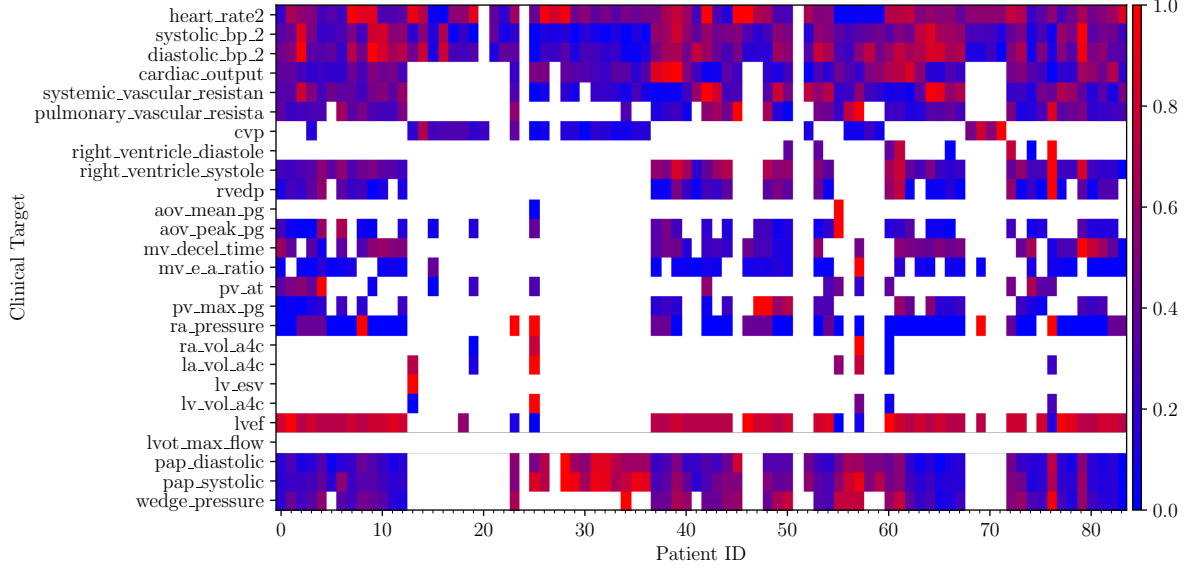


Figure 1: Missing data pattern in EHR dataset. Each row in the above heat map is normalized to a $[0, 1]$ range to highlight the relative magnitude of the clinical target across patients.

two clinical measurements, the diastolic pulmonary artery pressure ($p_{p,d}$) and the systolic artery pressure ($p_{p,s}$), i.e.

$$\text{hypertensive} = \begin{cases} 1, & \text{if } p_{p,m} = \frac{2}{3} \cdot p_{p,d} + \frac{1}{3} \cdot p_{p,s} > 20 \text{ mmHg} \\ 0, & \text{if } p_{p,m} = \frac{2}{3} \cdot p_{p,d} + \frac{1}{3} \cdot p_{p,s} \leq 20 \text{ mmHg.} \end{cases} \quad (5)$$

Medical information, including EHR data, is highly sensitive and may reveal patients' medical conditions and history, among others, if not properly protected for privacy. Sharing the data is not an option due to privacy concerns. Generating and releasing synthetic data is proposed as an alternative and is actively explored by researchers and in practice (Benaim et al., 2020; Dash et al., 2019; Rankin et al., 2020; the SHARED team, 2023; Yale et al., 2020).

3.2 Privacy-preserving Synthetic Data Generation through DP-NF

Figure 1 shows that the EHR dataset contains a considerable portion of missing values. Before synthetic data generation, we first imputed the missing values using the MICE package (v3.13.0) in R. The MICE package implements multivariate imputation by chained equations (Van Buuren and Groothuis-Oudshoorn, 2011), which draws, in an alternated fashion (as in a Gibbs' sampler), imputed values for the missing attribute $X_{\cdot,j}$ from the conditional distribution $p(X_{\cdot,j}|\theta_j, \mathbf{X}_{\cdot,-j})$ and parameters θ_j from its posterior distribution $p(\theta_j|\mathbf{X})$ for $j = 1, \dots, p$. $\mathbf{X}_{\cdot,-j}$ contains all variables in the data except for $X_{\cdot,j}$.

In the EHR data, seven attributes (cvp, aov_mean_pg, ra_vol_a4c, la_vol_a4c, lv_escv, lv_vol_a4c, and lvot_max_flow) have large fractions of missing values that range from 63% to 100%. These large fractions of missing data turned out to be problematic for MICE. For that reason, these seven attributes were not considered in the imputation and any subsequent analysis. We obtained 5 sets of imputed data and then split each

of the 5 imputed datasets into a training set and a testing set with 64 and 20 patients, respectively.

We used DP-NF for density estimation in each of the 5 imputed datasets using Algorithm 1. After computing the privacy-preserving density $p^*(\mathbf{x})$ (we use $*$ to represent private or sanitized quantities), we can generate synthetic data \mathbf{x}^* by first sampling from the base distribution $\mathbf{z}_0 \sim q_0$ and then use the learned NF map $F_{\lambda^*}(\mathbf{z}_0)$ to generate realizations from p^* . Though the algorithm is presented using the SGD framework, it can easily be extended for other gradient-based optimization such as RMSprop (Tieleman et al., 2012) and Adam (Kingma and Ba, 2014), by replacing the update $(\lambda^{*(t+1)} = \lambda^{*(t)} - \eta g^{*(t)})$ with their respective parameter update paradigms.

Algorithm 1 DP-NF for Density Estimation

Input: data set $\mathbf{x} = \{\mathbf{x}_1, \dots, \mathbf{x}_n\}$, initial parameter values $\lambda^{(0)}$ of NF $F_{\lambda}(\cdot)$ with base distribution q_0 , learning rate η , DP noise scale σ , subsampling rate r , clipping constant on gradient C , number of iterations T .

Output: privacy-preserving estimated density $p^*(\mathbf{x})$

for $t = 0, \dots, T$ **do**

 sub-sample $\mathbf{x}^{(t)}$ from \mathbf{x} with rate r ; let $b^{(t)}$ be the size of $\mathbf{x}^{(t)}$

for $\mathbf{x}_i \in \mathbf{x}^{(t)}$ **do**

 let $\mathbf{z}_i = F_{\lambda}^{-1}(\mathbf{x}_i)$

 obtain $l_i = -\log q_0(\mathbf{z}_i) - \log |\partial F_{\lambda} / \partial \mathbf{z}_i|$

 compute $\mathbf{g}_i^{(t)} = \nabla_{\lambda} l_i$

$\mathbf{g}_i^{(t)} \leftarrow \mathbf{g}_i^{(t)} / \max(1, \|\mathbf{g}_i^{(t)}\|_2 / C)$

end for

 obtain sanitized gradient $\mathbf{g}^{*(t)} = \left(\sum_{i=1}^{b^{(t)}} \mathbf{g}_i^{(t)} + \mathcal{N}(\mathbf{0}, \sigma^2 C^2 \mathbf{I}) \right) / b^{(t)}$

$\lambda^{*(t+1)} = \lambda^{*(t)} - \eta \mathbf{g}^{*(t)}$

end for

In the application of Algorithm 1 to the EHR data, we set $r = 0.5, \eta = 2 \times 10^{-5}, T = 8000, C = 10$. We examined 4 privacy budgets μ in the setting of μ -GDP, i.e., $\mu = (6.10, 3.92, 2.45, 1.49)^2$, corresponding to $\sigma = (7.36, 11.44, 18.28, 29.93)$ and $\epsilon = (32, 16, 8, 4)$ if $\delta = 0.01$ in the (ϵ, δ) -DP setting. The NF architecture we used has 15 MADE layers, each consisting of a fully connected neural network having 1 hidden layer with 200 neurons, and one batch normalization layer following each MADE. For each of the 5 imputed training sets, we run DP-NF 10 times to obtain 10 privacy-preserving densities; from each estimated density, 10 synthetic datasets were generated, leading to a total of 500 synthetic data sets³. Each synthetic data contains the same number of subjects (82) as in the original dataset.

We use the generated synthetic data for three subsequent learning and inferential tasks.

²We also attempted smaller μ (e.g. $\mu \leq 1$), but the DP-NF algorithm did not converge due to a large amount of noise injected to the gradients.

³We generated multiple data sets to examine the stability of the results in the downstream learning tasks in Sections 3.3 and 3.4. In practice, one may release multiple synthetic data to take into account the uncertainty around sanitization and synthesis, and then combine the inferences from multiple sets using the rule in Liu (2022). Correspondingly, the overall privacy budget needs to split across multiple sets when generating privacy-preserving synthetic data. For machine learning tasks based on synthetic data, releasing a single synthetic dataset may be sufficient.

The first two focus on detecting pulmonary hypertension and predicting the mean pulmonary arterial pressure from the testing data (Section 3.3), while the last conducts VI for the parameters of a physics-based model (Section 3.4).

3.3 Classification and Regression based on Privacy-preserving Synthetic EHR Data

The goal of this learning task is to detect pulmonary hypertension, defined as a mean pulmonary artery pressure $p_{p,m}$ greater than 20 mmHg in Eqn. (5). Toward that end, we train a binary classifier (hypertensive/not hypertensive) using support vector machine (SVM, Cortes and Vapnik, 1995) and a numerical estimate of the mean pulmonary artery pressure using a random forest (see, e.g., Breiman, 2001). We evaluated the classification and regression testing accuracy of these two procedures trained on the privacy-preserving synthetic data. SVM outputs a probability of having pulmonary hypertension for each case. Instead of using a cutoff of 0.5, we adopted the Fowlkes–Mallows (FM) index (Fowlkes and Mallows, 1983) to find an optimal cutoff. The FM index is defined as $\sqrt{\frac{TP}{TP+FP} \cdot \frac{TP}{TP+FN}}$, where TP is the number of true positives, FP is the number of false positives, and FN is the number of false negatives. The cutoff that produces the maximum FM index was used.

Tables 2 and 3 summarize the prediction results over the 500 synthetic datasets. Both tables present two sets of results, one based on SVM or random forest trained on the raw generated synthetic data, the other based on SVM or random forest trained on post-processed synthetic data by projecting an out-of-bound synthetic data point back to either its lower or upper bound. The reason for the post-processing is that the attributes in the EHR data are clinical attributes and they are naturally bounded. For example, the attribute “peak pressure gradient across pulmonary valve” relates to pulmonary valve stenosis; values outside $[0, 50]$ would be regarded as physiologically impossible for our EHR dataset which does not contain patients with pulmonary valve stenosis. Therefore, if a synthetic value on “peak PG across pulmonary valve” is < 0 mmHg, it is set at 0 and, is set at 50 mmHg if found > 50 mmHg.

Table 2: Privacy-preserving mean classification accuracy rate (SD) via SVM based on synthetic data generated via DP-NF

Truncation*	Imputation	Original	$\mu = \infty$	$\mu = 6.10$	$\mu = 3.92$	$\mu = 2.45$	$\mu = 1.49$
No	1	1.00	0.95 (0.07)	0.91 (0.08)	0.82 (0.24)	0.81 (0.15)	0.87 (0.09)
	2	1.00	0.88 (0.24)	0.93 (0.06)	0.86 (0.10)	0.88 (0.12)	0.83 (0.11)
	3	1.00	0.92 (0.09)	0.91 (0.06)	0.90 (0.08)	0.88 (0.10)	0.72 (0.38)
	4	0.95	0.89 (0.10)	0.88 (0.05)	0.80 (0.09)	0.76 (0.22)	0.86 (0.12)
	5	0.95	0.85 (0.20)	0.90 (0.07)	0.88 (0.17)	0.92 (0.17)	0.80 (0.10)
	mean	0.98	0.90 (0.16)	0.91 (0.07)	0.85 (0.15)	0.85 (0.20)	0.81 (0.20)
Yes	1	1.00	0.92 (0.08)	0.87 (0.09)	0.79 (0.24)	0.80 (0.15)	0.85 (0.09)
	2	1.00	0.83 (0.26)	0.89 (0.07)	0.86 (0.09)	0.86 (0.11)	0.83 (0.10)
	3	1.00	0.90 (0.11)	0.90 (0.07)	0.90 (0.08)	0.88 (0.10)	0.70 (0.37)
	4	0.95	0.85 (0.16)	0.87 (0.06)	0.80 (0.08)	0.74 (0.33)	0.82 (0.12)
	5	0.95	0.77 (0.28)	0.85 (0.08)	0.85 (0.17)	0.88 (0.17)	0.80 (0.10)
	mean	0.98	0.85 (0.20)	0.88 (0.08)	0.84 (0.15)	0.83 (0.20)	0.80 (0.20)

* Imputed and synthetic data on an attribute may exceed the physiologically feasible bounds. The results in “Truncation = Yes” are obtained based on post-processed imputed and synthetic data by setting the out-of-bound values at the closest bound.

Table 3: Privacy-preserving prediction mean squared error (SD) via random forest based on synthetic data generated via DP-NF

Truncation*	Imputation	Original	$\mu = \infty$	$\mu = 6.10$	$\mu = 3.92$	$\mu = 2.45$	$\mu = 1.49$
No	1	20.63	40.30 (23.37)	54.71 (20.20)	62.45 (20.55)	83.44 (42.54)	70.39 (30.52)
	2	18.02	35.70 (19.87)	48.08 (18.10)	60.06 (22.89)	62.44 (33.44)	80.30 (44.03)
	3	11.50	71.76 (62.20)	36.53 (7.39)	47.02 (23.01)	72.22 (28.51)	71.36 (30.02)
	4	18.87	32.92 (27.36)	44.15 (12.19)	63.09 (19.02)	46.81 (26.87)	60.52 (17.59)
	5	20.66	81.45 (59.57)	53.98 (17.75)	59.53 (29.41)	41.09 (18.28)	122.91 (41.70)
	mean	17.94	52.52 (47.18)	47.40 (17.17)	58.41 (23.86)	61.39 (34.49)	80.10 (39.92)
Yes	1	21.49	47.50 (27.68)	72.30 (23.98)	79.00 (26.64)	95.76 (43.68)	75.85 (28.33)
	2	18.54	47.08 (24.01)	56.77 (15.78)	68.91 (22.45)	73.43 (36.21)	88.21 (42.44)
	3	12.12	68.25 (55.06)	47.09 (12.74)	55.26 (22.01)	80.08 (29.44)	85.45 (29.94)
	4	18.06	35.55 (30.28)	55.24 (13.12)	71.30 (24.08)	51.26 (26.73)	66.17 (22.38)
	5	19.79	78.79 (53.02)	63.31 (18.31)	68.13 (31.79)	53.75 (21.02)	112.54 (40.61)
	mean	18.00	55.91 (42.61)	58.94 (19.23)	68.52 (26.77)	71.91 (35.70)	84.91 (36.52)

* Imputed and synthetic data on an attribute may exceed the physiologically feasible bounds. The results in “Truncation = Yes” are obtained based on post-processed imputed and synthetic data by setting the out-of-bound values at the closest bound.

Overall, as expected, the higher the privacy loss (larger μ), the higher the accuracy rates (Table 2) and the smaller the prediction MSE (Table 3). The post-processing truncation needed to enforce bounds for each clinical measurement satisfies the practical data constraints but negatively affects the prediction results; the accuracy rates decrease in Table 2 and the prediction MSE increases in Table 3 with truncation vs. without truncation, regardless of the preferred privacy budget; but the trend over μ is similar to that before the truncation.

3.4 VI of Parameters in Physics-based model using Privacy-preserving Synthetic EHR data

3.4.1 the CVSim-6 physiologic model

The evolution of blood pressure, flow, and volume in the circulatory system of an adult subject is simulated, in this study, using CVSim-6 (Davis, 1991; Heldt et al., 2010), a lumped parameter hemodynamic model with 6-compartments available through the PhysioNet repository (Goldberger et al., 2000). A custom Python/Cython implementation can be found at <https://github.com/desResLab/supplMatHarrod20>. The model includes compartments for the left heart, right heart, systemic arteries, systemic veins, pulmonary arteries and pulmonary veins. Arterial and venous compartments consist of RC circuits, while heart chambers are simulated using a pressure generator, two unidirectional diodes and a resistor to account for the pressure loss produced at the valves. All elements are considered linear, disregarding collapsibility in veins associated with negative pressures. Inertial effects are also assumed negligible (the model does not contain inductors) and a two-chamber heart is considered, disregarding any contribution from the atria. In addition, interaction is only considered between adjacent compartments. Thus, unlike other model formulations in the literature (see, e.g., CircAdapt, see Arts et al., 2005) no mechanical interaction is considered between the two ventricular chambers through the septal wall. CVSim-6 consists of a system of six differential equations (one per compartment). The flows between the compartments, under the assumption of nonlinear unidirectional valves (without regurgitation), are expressed as (see Davis, 1991,

Sections 4.2.1 and 4.2.2)

$$\begin{aligned}
q_{li} &= \begin{cases} (P_{pv} - P_l)/R_{li} & \text{if } P_{pv} > P_l \\ 0 & \text{otherwise} \end{cases} & q_{lo} &= \begin{cases} (P_l - P_a)/R_{lo} & \text{if } P_l > P_a \\ 0 & \text{otherwise} \end{cases} \\
q_{ri} &= \begin{cases} (P_v - P_r)/R_{ri} & \text{if } P_v > P_r \\ 0 & \text{otherwise} \end{cases} & q_{ro} &= \begin{cases} (P_r - P_{pa})/R_{ro} & \text{if } P_r > P_{pa} \\ 0 & \text{otherwise} \end{cases} , \quad (6) \\
q_a &= (P_a - P_v)/R_a & q_{pv} &= (P_{pa} - P_{pv})/R_{pv}
\end{aligned}$$

leading to the following differential equations for RC elements with fixed and time-varying capacitance

$$\begin{aligned}
\frac{dP_l}{dt} &= \frac{q_{li} - q_{lo} - (P_l - P_{th}) dC_l(t)/dt}{C_l(t)}, & \frac{dP_a}{dt} &= \frac{q_{lo} - q_a}{C_a}, \\
\frac{dP_v}{dt} &= \frac{q_a - q_{ri}}{C_v}, & \frac{dP_r}{dt} &= \frac{q_{ri} - q_{ro} - (P_r - P_{th}) dC_r(t)/dt}{C_r(t)}, \\
\frac{dP_{pa}}{dt} &= \frac{q_{ro} - q_{pv}}{C_{pa}}, & \frac{dP_{pv}}{dt} &= \frac{q_{pv} - q_{li}}{C_{pv}}.
\end{aligned} \quad (7)$$

Initial conditions are determined from a system of linear equilibrium equations on the stressed volume,

$$\begin{aligned}
C_{l,dias} (P_{l,dias} - P_{th}) - C_{l,sys} (P_{l,sys} - P_{th}) &= C_{r,dias} (P_{r,dias} - P_{th}) - C_{r,sys} (P_{r,sys} - P_{th}) \\
&= T_{sys} \frac{P_{l,sys} - P_a}{R_{lo}} = T_{tot} \frac{P_a - P_v}{R_a} \\
&= T_{dias} \frac{P_v - P_{r,dias}}{R_v} = T_{sys} \frac{P_{r,sys} - P_{pa}}{R_{ro}} \\
&= T_{tot} \frac{P_{pa} - P_{pv}}{R_{pv}} = T_{dias} \frac{P_{pv} - P_{l,dias}}{R_{li}} \\
V_{tot} - V_{0,tot} &= C_{l,dias} (P_{l,dias} - P_{th}) + C_a (P_a - \frac{1}{3} P_{th}) + \\
&\quad C_v P_v + C_r (P_r - P_{th}) + C_{pa} (P_{pa} - P_{th}) + \\
&\quad C_{pv} (P_{pv} - P_{th}).
\end{aligned} \quad (8)$$

The acronyms used in the equations above are defined in Table 8 in the Appendix. Default model parameters are reported in Table 4 and pressure, volume, and flow rate time histories produced by CVSim-6, when such parameters are used as inputs, are shown in Figure 2.

The CVSim-6 model is compactly represented as $\mathbf{x} = \mathbf{f}(\mathbf{z})$, where \mathbf{z} and \mathbf{x} represent the model inputs (parameters, either unknown or fixed at constants) and outputs (observed), respectively. A subset consisting of 8 outputs was in the construction of the likelihood function given the EHR data, including heart rate, pulmonary vascular resistance, central venous pressure, right ventricular diastolic pressure, right ventricular systolic pressure, right ventricle end-diastolic pressure, average pressure gradient across the aortic valve, and peak pressure gradient across the aortic valve. Such quantities are obtained by post-processing the time histories for the state and auxiliary variables shown in Figure 2. In this study, we regard right ventricular resistance R_{ro} and arterial capacitance C_a as unknown parameters (inputs to the model), whereas the other parameters are fixed to their default values in Table 4.

Table 4: Default parameters for CVSim-6 model (see Table 4.1 in Davis (1991))

Compartment	R_i (mmHg s/mL)	R_o (mmHg s/mL)	C (mL/mmHg)	V_0 (mL)
Left Heart	0.01	0.006	0.4-10	15
Systemic Arteries	0.006	1.00	1.6	715
Systemic Veins	1.00	0.05	100.0	2500.0
Right Heart	0.05	0.003	1.2-20	15
Pulmonary Arteries	0.003	0.08	4.3	90
Pulmonary Veins	0.08	0.01	8.4	490

Systemic parameters: total blood volume = 5000 mL, heart rate = 72 bpm; transthoracic pressure = -4.0 mmHg.

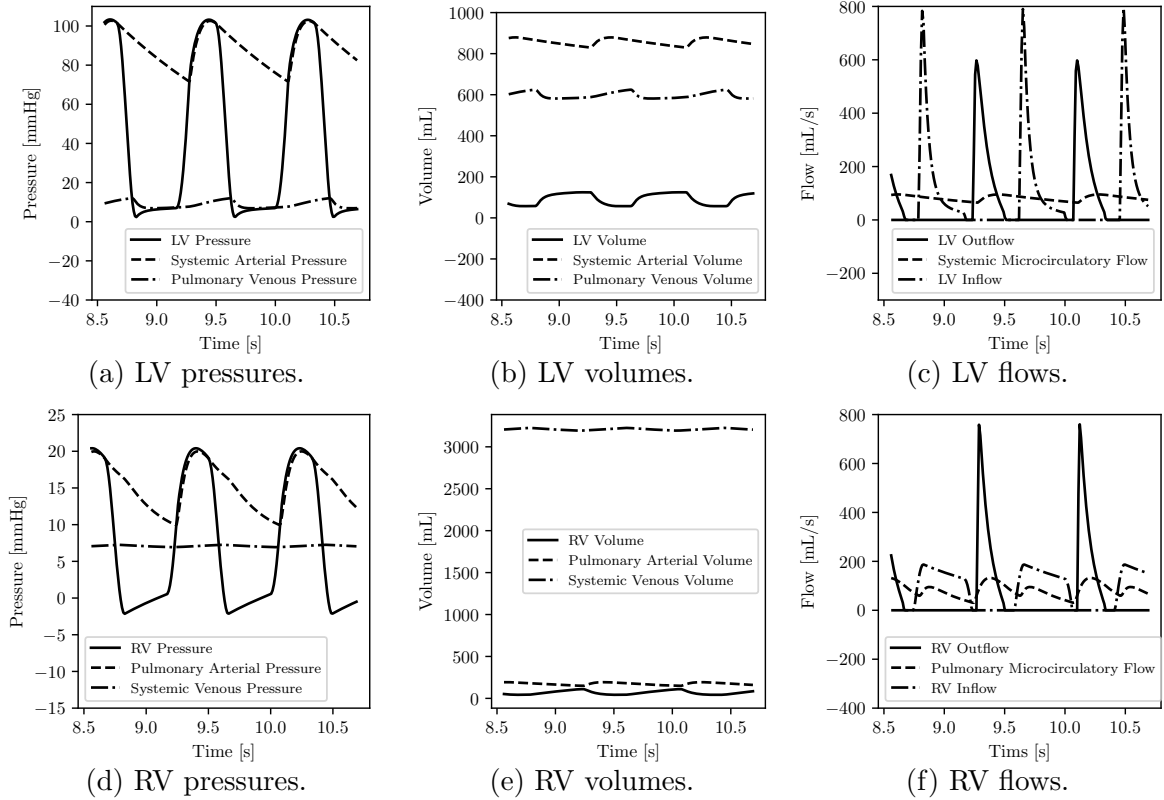


Figure 2: Time histories of state and auxiliary variables from CVSim-6 model, when using the default input parameters listed in Table 4 (see Figure 4-4 in Davis, 1991).

3.4.2 VI based on privacy-preserving synthetic EHR data

To infer the CVSim-6 model parameters R_{ro} and C_a for hypertensive patients, we construct the likelihood based on a subset of 43 synthetic hypertensive patients. We assume a uniform prior of the transformed parameters (R', C') on $[-7, 7]^2$,

$$(R_{ro}, C_a) = (\tanh(3/7 \cdot R') \cdot (H_R - L_R)/2 + R_0, \tanh(3/7 \cdot C') \cdot (H_C - L_C)/2 + C_0), \quad (9)$$

where $R_{ro} \in [L_R, H_R]$, $C_a \in [L_C, H_C]$ are the original parameters with respective bounds, R_0, C_0 are default values, and (R', C') are their transformed unbounded counterpart.

We assume the 8-dimensional output $\mathbf{x}_i = (x_{i,1}, \dots, x_{i,8})$, given the parameters (R_{ro}, C_a) , follows a multivariate Gaussian distribution. Assuming independence across the 8 outputs

with known marginal variance for each output, the log-likelihood of (R_{ro}, C_a) is

$$\ell(R_{ro}, C_a; \mathbf{x}) = -\frac{1}{2} \sum_{i=1}^n [\mathbf{x}_i - \mathbf{f}(R_{ro}, C_a)]^T \mathbf{\Sigma}^{-1} [\mathbf{x}_i - \mathbf{f}(R_{ro}, C_a)]^2 + \text{constant}, \quad (10)$$

where $\mathbf{f}(R_{ro}, C_a)$ represents the output of the CVSim-6 model with all but two input variables fixed at their default values and $\mathbf{\Sigma}$ is a diagonal matrix with marginal variances equal to (444.84, 145.60, 2.21, 45034.41, 475.59, 24.77, 84.06, 15.48) for the 8-dimensional output.

The CVSim-6 model is computationally expensive. To reduce the computational cost of VI with input parameters R_{ro} and C_a , we trained offline a fully connected neural network surrogate. The network contains 2 hidden layers with 64 and 32 neurons, respectively, and Tanh activations. We generated 100 realizations using Sobol’ sampling in the (R_{ro}, C_a) plane and computed the corresponding outputs from the CVSim-6 model. We then trained the surrogate model based on 100 sets of inputs (2-dimensional) and outputs (8-dimensional) in 120,000 iterations with the RMSprop optimizer (learning rate 0.01, learning rate scheduler with exponential decay factor 0.9999) using a ℓ_2 loss with ℓ_2 regularization (penalty 0.0001).

We train the surrogate model and run NF to obtain posterior distribution on the transformed (R', C') first, which are then transformed back to obtain the posterior distribution and VI of R_{ro}, C_a . VI was performed using a MAF architecture with 5 alternated MADE and batch normalization layers. Each MADE uses a fully connected neural network characterized by 1 hidden layer with 100 neurons. The activation functions within and between successive MADE layers are ReLU. The network is trained for 15,000 iterations, generating batches of 500 samples at each iteration. We use RMSProp as the optimizer with a learning rate of 0.01 and an exponential scheduler with a decay rate of 0.9999.

VI results for R_{ro} and C_a based on the privacy-preserving synthetic data are presented in Table 5, showing the posterior mean and posterior standard deviations of the two parameters, and the correlations between them across 5 different imputations. In summary, the estimates based on privacy-preserving synthetic data are somewhat different from those based on the original data and there does not appear to be an obvious trend over μ in terms of how the former differs from the latter, except for the posterior correlation between R_{ro} and C_a , which appears to get more negative as μ , the privacy loss, decreases.

Table 5: Privacy-preserving VI for CVSim-6 model parameters R_{ro} and C_a based on synthetic data generated via DP-NF

parameter	posterior estimate	original	$\mu = 6.10$	$\mu = 3.92$	$\mu = 2.45$	$\mu = 1.49$
R_{ro}	mean	35.70 (1.918)	43.83 (2.798)	45.90 (2.788)	47.52 (4.400)	45.61 (3.748)
	SD	1.452 (0.038)	1.907 (0.032)	2.168 (0.341)	2.189 (0.383)	2.144 (0.165)
C_a	mean ($\times 10^{-4}$)	6.520 (0.130)	8.569 (1.169)	8.345 (1.647)	7.972 (0.967)	8.917 (1.023)
	SD ($\times 10^{-4}$)	0.347 (0.013)	0.609 (0.135)	0.666 (0.362)	0.594 (0.200)	0.724 (0.192)
R_{ro}, C_a correlation		-0.120 (0.042)	-0.123 (0.192)	-0.169 (0.275)	-0.213 (0.244)	-0.193 (0.164)

Figure 3 presents the scatter plots of the posterior samples on R_{ro} and C_a from the NF run on one private synthetic dataset. The observations are consistent with those in Table 5. In general, the posterior samples generated from the NF constructed from

the privacy-preserving synthetic data are located near the high-density regions of the posterior distribution based on the original data and true model, though not quite around the mode, and the mild negative correlation between the two parameters is also roughly retained for $\mu \geq 2.45$. There is more dispersion among the posterior samples at all μ , especially at $\mu = 1.49$, due to the noise injected to achieve DP guarantees, as expected.

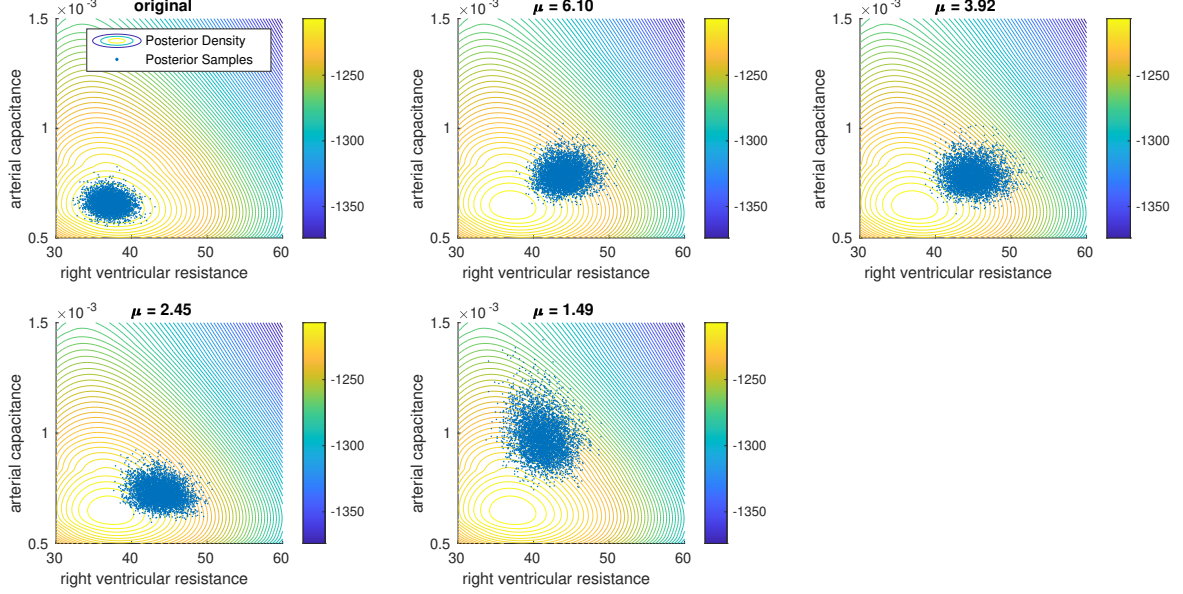


Figure 3: Example of privacy-preserving posterior samples of R_{ro} and C_a through MAF based on one synthetic dataset. The contours are the densities of the true posterior distribution of R_{ro} and C_a given the true model and the original data.

4 Privacy-Preserving VI via DP-NF

In this section, we examine the feasibility of privacy-preserving VI through sanitization of the optimization procedure employed by NF for VI, referred as the DP-NF-VI Procedure for short. Though NF can be used for both density estimation and VI and gradient-based optimization can be used to obtain the respective solutions in both cases, the loss functions in the two cases are different (likelihood in Eqn. (3) vs. free energy bound in Eqn. (4)). In what follows, we first provide an algorithm for DP-NF-VI with DP guarantees for NF-VI and then examine the inferential utility of privacy-preserving VI via DP-NF in simulated data.

4.1 The DP-NF-VI Procedure

The steps of the DP-NF-VI Procedure is given in Algorithm 2. Similar to Algorithm 1, Algorithm 2 is obtained from an SGD optimizer by clipping and perturbing the gradient with additive noise; and it can easily be extended to other gradient-based optimization procedures such as RMSprop or Adam by replacing the parameter updating step ($\lambda^{*(t+1)} = \lambda^{*(t)} - \eta g^{*(t)}$) with their respective parameter update paradigms. The differences between the two algorithms are in the loss function and the privacy-preserving output which are the free energy and the privacy-preserving variational density approximation $p^*(\mathbf{z})$, respectively, in Algorithm 1. We can draw samples from privacy-preserving samples of \mathbf{z} from $p^*(\mathbf{z})$ by first generating $\mathbf{z}_0 \sim q_0$ and then applying the transformation $F_{\lambda^*}(\mathbf{z}_0)$.

Algorithm 2 The DP-NF-VI Procedure

Input: observed data $\mathbf{x} = \{\mathbf{x}_1, \dots, \mathbf{x}_n\}$, target posterior distribution $p(\mathbf{z}|\mathbf{x})$, NF $F_\lambda(\mathbf{z}) = f_K \circ f_{K-1} \circ \dots \circ f_1(\mathbf{z})$ with base distribution q_0 , initial values $\lambda^{(0)}$, learning rate η , DP noise scale σ , sub-sampling rate r , gradient clipping constant C , number of iterations T , batch size m .

Output: privacy-preserving variational distribution $p^*(\mathbf{z})$.

for $t = 0, \dots, T$ **do**

 sub-sample $\mathbf{x}^{(t)}$ from \mathbf{x} with rate r ; let $b^{(t)}$ denote the size of $\mathbf{x}^{(t)}$

 draw m samples from $\mathbf{z}_0 \sim q_0$

for $\mathbf{x}_i \in \mathbf{x}^{(t)}$ **do**

$l_i(\lambda) = m^{-1} \sum_{j=1}^m \{n^{-1} \log q_0(\mathbf{z}_{0,j}) - \log p(\mathbf{x}_i, F_\lambda(\mathbf{z}_{0,j})) - n^{-1} \log |\partial F_\lambda / \partial \mathbf{z}_{0,j}|\}$

 obtain $\mathbf{g}_i^{(t)} = \nabla_\lambda l_i(\lambda)$ and $\mathbf{g}_i^{(t)} \leftarrow \mathbf{g}_i^{(t)} / \max(1, \|\mathbf{g}_i^{(t)}\|_2 / C)$

end for

 obtain sanitized gradient $\mathbf{g}^{*(t)} = \left(\sum_{i=1}^{b^{(t)}} \mathbf{g}_i^{(t)} + \mathcal{N}(\mathbf{0}, \sigma^2 C^2 \mathbf{I}) \right) / b^{(t)}$

$\lambda^{*(t+1)} = \lambda^{*(t)} - \eta \mathbf{g}^{*(t)}$

end for

4.2 Application of DP-NF-VI to Simulated Data

We used a simulated dataset⁴ to evaluate the utility of VI obtained via Algorithm 2. Specifically, we simulated outputs \mathbf{x} as given covariates \mathbf{w} and model parameters $\boldsymbol{\beta}$ from the following nonlinear model

$$x_{i,k} = f(\mathbf{w}_i, \boldsymbol{\beta}) + r_i + e_{i,k}, \quad (11)$$

where

$$f(\mathbf{w}_i, \boldsymbol{\beta}) = \beta_0 + \exp[\beta_1 w_{i,1}] + \log[w_{i,2} + \exp(\beta_2)] + \exp[\beta_2 w_{i,3}] + \log[w_{i,4} + \exp(\beta_4)], \quad (12)$$

and, additionally,

$$r_i \sim \mathcal{N}(0, \sigma_0^2), \quad e_{i,k} \sim \mathcal{N}(0, \sigma^2), \quad (13)$$

for $i = 1, \dots, 6000$ and $k = 1, \dots, 5$. The covariates \mathbf{w} were generated using $w_{i,j} \sim \mathcal{U}(0, a_j)$ independently with $i = 1, \dots, n$ and $a_1 = 1, a_2 = 3, a_3 = 0.5, a_4 = 2$. We set $\sigma_0 = \sigma = 0.2$ and $\boldsymbol{\beta} = (0.2, 1.0, 0.8, -1.2, 0.6)^T$. The random effect r_i introduces correlation among 5 repeated measurements observed for the i -th subject, where the correlation is $\sigma^2 / (\sigma^2 + \sigma_0^2) = 1/2$.

Our goal is to estimate a privacy-preserving posterior distribution of $\boldsymbol{\beta}$ and obtain its privacy-preserving posterior inference given a non-informative uniform prior $p(\boldsymbol{\beta})$ and the likelihood $l(\boldsymbol{\beta}|\mathbf{x})$, where, WLOG, σ_0^2, σ^2 are assumed known. We applied Algorithm 2 to the simulated data at various levels of μ -GDP guarantees ($\mu = 6.58, 1.12, 0.5$ and 0.27 , which correspond to $\epsilon = 50, 5, 2, 1$ when $\delta = 1 \times 10^{-5}$). We used a MAF architecture with one MADE (1 hidden layer with 10 neurons) and one batch norm layer. We also used a batch of size $m = 1,000$ to compute the Monte Carlo estimates of the loss function in Algorithm 2, a sub-sampling rate $r = 500/6,000$, learning rate $\eta = 0.01$ with exponential scheduler decay factor 0.999, number of iterations $T = 8,000$, and clipping constant $C = 10.0$.

⁴We also ran the algorithm on the EHR dataset but it failed to converge.

The results on the privacy-preserving posterior inference for β are reported in Table 6. In summary, the privacy-preserving posterior means remain roughly constant regardless of the selected privacy loss parameter μ , whereas the SD values in the parentheses are greater than the corresponding non-private values (column “original VI NF”), and become increasingly larger when μ decreases. Additionally, the private correlations among different elements of β computed using DP-NF-VI are in general more pronounced with respect to the corresponding original values and are associated with large SDs from the 5 different DP-NF-VI runs, indicating a general lack of stability for these estimates.

Table 6: Differentially private VI on the nonlinear regression model parameters β from DP-NF-VI (Algorithm 2).

parameter	original nonlinear model	original NF-VI	$\mu = 6.68$ $\sigma = 1.30$	$\mu = 1.12$ $\sigma = 6.68$	$\mu = 0.50$ $\sigma = 14.88$	$\mu = 0.27$ $\sigma = 27.82$
Posterior Mean						
β_0 (0.2)	0.1581	0.1593 (0.0020)	0.1532 (0.0035)	0.1381 (0.0151)	0.1231 (0.0486)	0.1419 (0.0701)
β_1 (1.0)	1.0022	1.0016 (0.0015)	0.9952 (0.0040)	0.9957 (0.0036)	0.9922 (0.0059)	0.9943 (0.0026)
β_2 (0.8)	0.8262	0.8265 (0.0013)	0.8386 (0.0034)	0.8404 (0.0150)	0.8378 (0.0208)	0.8584 (0.0278)
β_3 (-1.2)	-1.1909	-1.1920 (0.0008)	-1.1928 (0.0019)	-1.1891 (0.0079)	-1.1822 (0.0201)	-1.1945 (0.0246)
β_4 (0.6)	0.6088	0.6092 (0.0006)	0.6100 (0.0010)	0.6215 (0.0057)	0.6311 (0.0390)	0.6057 (0.0479)
Posterior SD						
β_0	0.0265	0.0255 (0.0011)	0.1341 (0.0147)	0.2576 (0.0241)	0.2573 (0.0490)	0.2791 (0.0825)
β_1	0.0036	0.0036 (0.0001)	0.1089 (0.0884)	0.0687 (0.0587)	0.1344 (0.1247)	0.0554 (0.0058)
β_2	0.0179	0.0174 (0.0008)	0.0755 (0.0222)	0.1267 (0.0250)	0.1729 (0.0309)	0.1655 (0.0305)
β_3	0.0151	0.0151 (0.0004)	0.0812 (0.0056)	0.1341 (0.0141)	0.1644 (0.0203)	0.1581 (0.0217)
β_4	0.0192	0.0191 (0.0006)	0.0889 (0.0163)	0.1197 (0.0089)	0.1595 (0.0384)	0.2012 (0.0399)
Posterior Correlation						
β_0, β_1	-0.1200	-0.0319 (0.0499)	-0.1147 (0.2240)	-0.1230 (0.2623)	0.0237 (0.1028)	-0.1619 (0.2592)
β_0, β_2	-0.4340	-0.3415 (0.1899)	-0.1180 (0.5120)	-0.3923 (0.4756)	0.0396 (0.3675)	-0.3269 (0.7675)
β_0, β_3	-0.7370	-0.7550 (0.0127)	-0.9108 (0.0851)	-0.8923 (0.0353)	-0.8629 (0.0407)	-0.8622 (0.0420)
β_0, β_4	-0.4880	-0.4883 (0.0356)	-0.5299 (0.4673)	-0.8545 (0.0839)	-0.6826 (0.1586)	-0.4920 (0.5249)
β_1, β_2	-0.0030	-0.0082 (0.0417)	-0.0310 (0.5503)	0.0285 (0.0406)	0.0916 (0.1965)	-0.0395 (0.1101)
β_1, β_3	-0.0160	-0.0892 (0.0264)	0.1255 (0.2115)	-0.0381 (0.2270)	-0.1815 (0.1485)	-0.0691 (0.2162)
β_1, β_4	-0.0080	-0.0680 (0.0252)	-0.2880 (0.4993)	0.1445 (0.2869)	-0.0457 (0.0595)	0.0784 (0.2416)
β_2, β_3	0.0040	-0.0538 (0.1526)	-0.0947 (0.6286)	0.1131 (0.4442)	-0.2520 (0.4011)	0.1453 (0.7946)
β_2, β_4	-0.0020	-0.0836 (0.0936)	-0.2267 (0.4445)	0.3336 (0.5772)	-0.2036 (0.2303)	-0.0271 (0.5412)
β_3, β_4	-0.0020	0.0318 (0.0443)	0.3368 (0.3616)	0.6469 (0.1602)	0.4218 (0.0884)	0.2300 (0.5860)

The results were averaged over 5 runs of DP-NF-VI; the SD values over the 5 runs in the parentheses.

As a comparison, we also performed VI for β in the nonlinear model based on privacy-preserving synthetic data generated using DP-NF for density estimation (Algorithm 1). For this task, we use a MAF architecture consisting of one MADE (1 hidden layer, 10 neurons) and one batch norm layer. We also used RMSprop with a batch size of 500, a learning rate of 0.01, and an exponential learning rate scheduler with a decay factor equal to 0.999. The total number of iterations was set to 8,000 and the gradient clipping constant C to 10.0.

The results are presented in Table 7. In general, regardless of μ , the posterior estimates of β from NF-VI based on privacy-preserving synthetic data show superior accuracy and are more similar to the results from non-private inference than those obtained directly from DP-NF-VI (Table 6). In addition, the SD values in the parentheses across multiple sets of synthetic data are relatively small, while the posterior correlations β are reasonably close to their original non-private values.

Table 7: Privacy-preserving VI based on synthetic data generated via DP-NF for density estimation (Algorithm 1).

parameter	original nonlinear model	original NF	$\mu = 6.68$ $\sigma = 1.30$	$\mu = 1.12$ $\sigma = 6.68$	$\mu = 0.50$ $\sigma = 14.88$	$\mu = 0.27$ $\sigma = 27.82$
Posterior Mean						
β_0 (0.2)	0.1581	0.1593 (0.0020)	0.1632 (0.0146)	0.1062 (0.0505)	0.0866 (0.0127)	0.0448 (0.0600)
β_1 (1.0)	1.0022	1.0016 (0.0015)	0.9891 (0.0060)	0.9943 (0.0060)	0.9917 (0.0097)	0.9775 (0.0126)
β_2 (0.8)	0.8262	0.8265 (0.0013)	0.8235 (0.0078)	0.8357 (0.0286)	0.8246 (0.0230)	0.8294 (0.0515)
β_3 (-1.2)	-1.1909	-1.1920 (0.0008)	-1.1807 (0.0081)	-1.1630 (0.0251)	-1.1406 (0.0138)	-1.1034 (0.0225)
β_4 (0.6)	0.6088	0.6092 (0.0006)	0.6011 (0.0230)	0.6261 (0.0237)	0.6197 (0.0145)	0.6214 (0.0233)
Posterior SD						
β_0	0.0265	0.0255 (0.0011)	0.0280 (0.0004)	0.0279 (0.0003)	0.0277 (0.0006)	0.0274 (0.0004)
β_1	0.0036	0.0036 (0.0001)	0.0040 (0.0000)	0.0040 (0.0000)	0.0039 (0.0001)	0.0038 (0.0001)
β_2	0.0179	0.0174 (0.0008)	0.0201 (0.0003)	0.0210 (0.0005)	0.0207 (0.0013)	0.0203 (0.0017)
β_3	0.0151	0.0151 (0.0004)	0.0159 (0.0003)	0.0153 (0.0002)	0.0144 (0.0007)	0.0142 (0.0006)
β_4	0.0192	0.0191 (0.0006)	0.0208 (0.0002)	0.0229 (0.0003)	0.0247 (0.0020)	0.0250 (0.0020)
Posterior Correlation						
β_0, β_1	-0.1200	-0.0319 (0.0499)	-0.0590 (0.0262)	-0.0568 (0.0130)	-0.0647 (0.0338)	-0.0359 (0.0185)
β_0, β_2	-0.4340	-0.3415 (0.1899)	-0.4184 (0.0159)	-0.4155 (0.0378)	-0.4588 (0.0606)	-0.4774 (0.0296)
β_0, β_3	-0.7370	-0.7550 (0.0127)	-0.7293 (0.0050)	-0.6919 (0.0092)	-0.6951 (0.0200)	-0.7049 (0.0326)
β_0, β_4	-0.4880	-0.4883 (0.0356)	-0.5206 (0.0103)	-0.5418 (0.0122)	-0.5168 (0.0315)	-0.4835 (0.0388)
β_1, β_2	-0.0030	-0.0082 (0.0417)	-0.0289 (0.0211)	-0.0244 (0.0196)	-0.0315 (0.0297)	-0.0774 (0.0207)
β_1, β_3	-0.0160	-0.0892 (0.0264)	-0.0723 (0.0285)	-0.0674 (0.0176)	-0.0607 (0.0249)	-0.0557 (0.0267)
β_1, β_4	-0.0080	-0.0680 (0.0252)	-0.0269 (0.0204)	-0.0318 (0.0166)	-0.0229 (0.0198)	-0.0428 (0.0171)
β_2, β_3	0.0040	-0.0538 (0.1526)	-0.0202 (0.0194)	-0.0409 (0.0257)	0.1278 (0.2343)	0.2144 (0.2168)
β_2, β_4	-0.0020	-0.0836 (0.0936)	-0.0346 (0.0156)	-0.0518 (0.0347)	-0.1289 (0.0761)	-0.1792 (0.0979)
β_3, β_4	-0.0020	0.0318 (0.0443)	0.0484 (0.0110)	0.0316 (0.0170)	-0.0257 (0.0677)	-0.0676 (0.0510)
The results were averaged over 5 sets of synthetic data generated via DP-NF for density estimation; the SD values in the parentheses are computed over the 5 sets.						

4.3 Further Utility Analysis of DP-NF-VI

The unsatisfactory results on the posterior correlations among the parameters, as displayed in Table 6, are not accidental. We tested the DP-NF-VI algorithm in multiple experiments on different datasets, and similar results were observed. We conjecture that this might be due to the usage of the free energy bound as the loss function in DP-NF-VI. Minimizing the free energy bound in NF-VI is equivalent to minimizing the KL divergence between the true posterior and its variational approximation. As a result of noise injection and gradient clipping in differentially private gradient-based optimization to achieve DP guarantees, the posterior variances of the parameters are expected to increase in the privacy-preserving variational distribution relative to those in the non-private target distribution. Thus, the DP-NF-VI procedure looks for densities in the variational family that are the most similar to the true posterior measured by the KL divergence but have larger variances. This may lead to an optimal variational density with a different correlation structure than the original.

To further demonstrate this phenomenon and test our conjecture, we run the following experiment. Despite the simplicity of the experiment, the results are interesting and insightful. Suppose the *target* distribution is a bivariate Gaussian distribution

$$p = \mathcal{N}(\mathbf{0}, \Sigma_0), \text{ with } \Sigma_0 = \sigma_0^2 [(1 - \rho_0)\mathbf{I}_{2 \times 2} + \rho_0 \mathbf{1}_{2 \times 2}].$$

We aim to approximate the distribution by another bivariate Gaussian distribution

$$q = \mathcal{N}(\mathbf{0}, \Sigma), \text{ with } \Sigma = \sigma^2 [(1 - \rho) \mathbf{I}_{2 \times 2} + \rho \mathbf{1}_{2 \times 2}],$$

which can be regarded as the *private* distribution, expected to have a larger marginal variance in each dimension compared to those in p ; i.e., $\sigma > \sigma_0$. We examine the following four dissimilarity (or divergence) metrics between p and q

$$L(p, q) = \begin{cases} \text{KL divergence} & D(q||p), \\ \text{reversed KL divergence} & D(p||q), \\ \ell_1 \text{ distance}^5 & \|q - p\|_1 = \int_{\mathbb{R}^2} |p(\mathbf{x}) - q(\mathbf{x})| d\mathbf{x}, \\ \text{Wasserstein distance} & W_\alpha(p, q) = (\inf_{\gamma \in \Gamma(p, q)} \mathbb{E}_\gamma |p - q|^\alpha)^{1/\alpha}. \end{cases}.$$

In this experiment, the Wasserstein distance is computed as

$$W_2(p, q) = \text{trace}(\Sigma_0 + \Sigma - 2[\Sigma^{1/2} \Sigma_0 \Sigma^{1/2}]^{1/2}).$$

We computed the dissimilarity between p and q (loss function) for each of the 4 metrics above as a function of ρ and σ and generated the corresponding contour plots in Figure 4, for three pairs (ρ_0, σ_0) at $(0, 1)$, $(1/2, 1)$ and $(1/2, 4)$, respectively. We then identified the value of ρ that minimizes the dissimilarity given an inflated standard deviation $\sigma = \hat{\sigma}$; that is,

$$\rho^*(\hat{\sigma}) = \arg \min_\rho L(\rho_0, \sigma_0, \rho, \hat{\sigma}),$$

The results of the experiment in Figure 4 suggest that the correlation ρ of the private distribution with *inflated* variance ($\sigma > \sigma_0$) that optimally approximates the target distribution (in the sense of minimal dissimilarity) depends, in general, on both ρ_0 and the selected dissimilarity metric.

When $\rho_0 = 0$, the optimal private approximation determined through both the KL divergence and the Wasserstein distance correctly matches the target correlation, i.e., $\rho = 0$; if the reverse KL divergence or the ℓ_1 distance is used, the optimal private approximation is not even unique, until its marginal variance σ is sufficiently close or smaller than σ_0 .

When ρ_0 is not 0, the optimal private approximation with inflated variance is characterized by a correlation ρ that rapidly tends to 1.0 as the inflation ratio σ/σ_0 increases. This behavior is observed in the cases of the KL divergence, the reverse KL divergence, and the ℓ_1 distance. However, the Wasserstein distance is still able to produce a private approximation with $\rho = \rho_0$ independently of the inflated variance σ .

In conclusion, the Wasserstein distance appears to be the best metric to use if one aims to preserve the correlation structure among the estimated parameters in private variational distributions, even with inflated marginal variance resulting from noise injection to achieve privacy guarantees.

5 Discussion

We examined the feasibility and utility of generating synthetic data via privacy-preserving NF for density estimation, with an application to an EHR dataset. Overall, the results

⁴Equivalent to twice the total variation norm $\|q - p\|_{TV} = \sup_{A \subset \mathbb{R}^2} |p(A) - q(A)|$

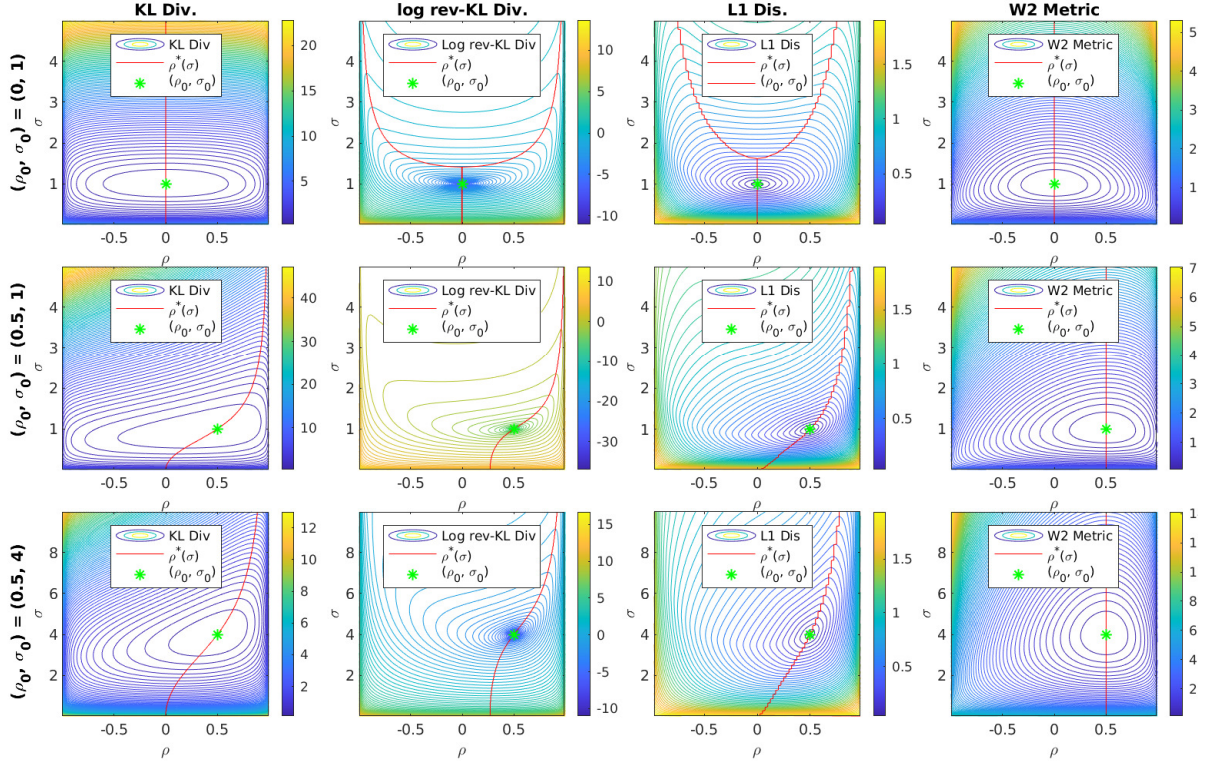


Figure 4: KL Divergence, reversed KL divergence, ℓ_1 and Wasserstein distance between *target* distribution $p = \mathcal{N}(\mathbf{0}, \Sigma_0)$ and its *private* approximation $q = \mathcal{N}(\mathbf{0}, \Sigma)$. The red line in contour plots is the trajectory of $\rho^*(\hat{\sigma}) = \arg \min_{\rho} L(\rho_0, \sigma_0, \rho, \hat{\sigma})$ that minimizes loss function L given $\hat{\sigma}$.

suggest that the downstream learning (prediction) and inferential procedure (VI) based on the privacy-preserving synthetic data can yield results of satisfactory and acceptable utility at practically reasonable choices of privacy loss parameters for the dataset. Though more empirical studies will be needed, this study on a real dataset with a relatively small sample size and a relatively large number of attributes of mixed types and missing values, suggests generating synthetic data via privacy-preserving NF for density estimation may be a practically feasible option for releasing and sharing sensitive information.

We also examined the feasibility of directly sanitizing the NF-VI procedure to generate privacy-preserving posterior inference. We show that the free energy bound as the loss function for NF-VI may yield variational distribution deviating significantly from the target distribution. This implies that alternative loss functions may better preserve the information on certain aspects of the target distribution, e.g., its correlation structure. In this context, we plan to further explore how the use of different distance metrics affects the performance of algorithms for DP-NF-VI, as a way to develop more effective strategies leveraging, for example, Wasserstein distance-based loss formulations.

The code for both the density estimation and VI through DP-NF is available on Github at <https://github.com/cedricwangyu/DPNF>.

Acknowledgements

This work is supported by an NSF Big Data Science & Engineering grant #1918692 (PI DES),

an NSF CAREER grant #1942662 (PI DES), an NSF OAC CDS&E grant #2104831 (Notre Dame PI DES) and used computational resources provided through the Center for Research Computing at the University of Notre Dame.

Appendix

A. Compliance With Ethical Standards

The EHR dataset utilized in this work contains data from external studies that involved human participants. The medical procedures that occurred in these studies were performed in accordance with both the ethical standards of the institutional and national research committee and with the 1964 Helsinki declaration and its later amendments. This study is classified as research not involving human subjects and was approved on June 13th, 2019, by the Office of Research Compliance and Institutional Review Board at the University of Notre Dame under IRB#19-05-5371.

B. Acronyms in CVSim-6 model

Table 8: Acronyms in CVSim-6 model

Flows			
q_{li}	Left ventricular inflow	q_{lo}	Left ventricular outflow
q_{ri}	Right ventricular inflow	q_a	Systemic aortic flow
q_{ro}	Right ventricular outflow	q_{pv}	Pulmonary venous flow
Pressures			
P_{pv}	Pulmonary venous pressure	P_l	Left ventricular pressure
P_a	Systemic arterial pressure	P_v	Systemic venous pressure
P_r	Right ventricular pressure	P_{pa}	Pulmonary arterial pressure
P_{th}	Thransthoracic pressure	$P_{r,dias}$	Right ventricular diastolic pressure
$P_{r,sys}$	Right ventricular systolic pressure	$P_{l,dias}$	Left ventricular diastolic pressure
$P_{l,sys}$	Left ventricular systolic pressure		
Resistances			
R_a	Systemic arterial resistance	$R_v = R_{ri}$	Systemic venous resistance
R_{lo}	Aortic valve resistance	R_v	Systemic venous resistance
R_{ro}	Pulmonary valve resistance	$R_{pv} = R_{li}$	Pulmonary venous resistance
Capacitances			
$C_l(t)$	Left ventricular capacitance	$C_r(t)$	Right ventricular capacitance
C_a	Systemic arterial capacitance	C_v	Systemic venous capacitance
C_{pa}	Pulmonary arterial capacitance	C_{pv}	Pulmonary venous capacitance
$C_{l,dias}$	Diastolic left ventricular capacitance	$C_{l,sys}$	Systolic left ventricular capacitance
$C_{r,dias}$	Diastolic right ventricular capacitance	$C_{r,sys}$	Systolic
Times			
T_{tot}	Total heart cycle time	T_{dias}	Duration of diastolic phase
T_{sys}	Duration of systolic phase		
Volumes			
V_{tot}	Total blood volume	$V_{0,tot}$	Unstressed blood volume

C. Hyper-parameters

We list the hyper-parameters used in all of our experiments in Table 9. EHR DP-DE indicates the differentially private density estimation in the EHR data (see Sec 3.2); EHR VI means VI with KL divergence in the privacy-preserving synthetic EHR data (see Sec 3.4.2); Reg DP-VI

represents differentially private VI in the simulated data via the nonlinear regression model (see Sec 4.2); Reg DP-DE means differentially private density estimation of the simulated data (see Sec 4.2); Reg VI means VI with KL divergence in the privacy-preserving simulated data 1 (See Sec 4.2). Except for the surrogate model (a fully connected neural network) for the CVSim-6 model, where the activation function tanh was used, ReLU was the activation function in all other NF and neural networks.

Table 9: Hyper-parameters used in all the experiments

parameter	EHR DP-DE	EHR VI	Reg DP-VI	Reg DP-DE	Reg VI
block No.	15	5	1	18	1
hidden No.	1	1	1	1	1
hidden size	200	100	10	100	10
input size	19	2	5	9	5
iter No.	8000	15000	8000	8000	8000
batch size	100	500	1000	100	1000
optimizer	SGD	RMSProp	RMSProp	RMSProp	RMSProp
learn rate	0.00002	0.01	0.01	0.002	0.01
scheduler	-	Exp	Exp	Exp	Exp
decay factor	-	0.9999	0.999	0.9995	0.999
clipping	10	-	10	5	-
poisson rate	50%	-	8.33%	8.33%	-

References

- M. Abadi, A. Chu, I. Goodfellow, H. B. McMahan, I. Mironov, K. Talwar, and L. Zhang. Deep learning with differential privacy. In *Proceedings of the 2016 ACM SIGSAC Conference on Computer and Communications Security*, pages 308–318, 2016.
- C. C. Aggarwal and P. S. Yu. A general survey of privacy-preserving data mining models and algorithms. In *Privacy-preserving data mining*, pages 11–52. Springer, 2008.
- F. Alda and B. I. Rubinstein. The Bernstein mechanism: Function release under differential privacy. In *Thirty-First AAAI Conference on Artificial Intelligence*, 2017.
- T. Arts, T. Delhaas, P. Bovendeerd, X. Verbeek, and F. W. Prinzen. Adaptation to mechanical load determines shape and properties of heart and circulation: the CircAdapt model. *American Journal of Physiology-Heart and Circulatory Physiology*, 288(4):H1943–H1954, 2005.
- M. Backes, P. Berrang, M. Humbert, and P. Manoharan. Membership privacy in microrna-based studies. In *Proceedings of the 2016 ACM SIGSAC Conference on Computer and Communications Security*, pages 319–330, 2016.
- B. K. Beaulieu-Jones, Z. S. Wu, C. Williams, R. Lee, S. P. Bhavnani, J. B. Byrd, and C. S. Greene. Privacy-preserving generative deep neural networks support clinical data sharing. *Circulation: Cardiovascular Quality and Outcomes*, 12(7):e005122, 2019.
- A. R. Benaim, R. Almog, Y. Gorelik, I. Hochberg, L. Nassar, T. Mashiach, M. Khamaisi, Y. Lurie, Z. S. Azzam, J. Khoury, et al. Analyzing medical research results based on synthetic data and their relation to real data results: systematic comparison from five observational studies. *JMIR medical informatics*, 8(2):e16492, 2020.

- C. M. Bowen and F. Liu. Comparative study of differentially private data synthesis methods. *Statistical Science*, 35(2):280–307, 2020.
- L. Breiman. Random forests. *Machine learning*, 45(1):5–32, 2001.
- Z. Bu, J. Dong, Q. Long, and W. J. Su. Deep learning with Gaussian differential privacy. *Harvard data science review*, 2020(23), 2020.
- M. Bun and T. Steinke. Concentrated differential privacy: Simplifications, extensions, and lower bounds. In *Theory of Cryptography Conference*, pages 635–658. Springer, 2016.
- M. Bun, C. Dwork, G. N. Rothblum, and T. Steinke. Composable and versatile privacy via truncated CDP. In *Proceedings of the 50th Annual ACM SIGACT Symposium on Theory of Computing*, pages 74–86, 2018.
- C. Butucea, A. Dubois, M. Kroll, and A. Saumard. Local differential privacy: Elbow effect in optimal density estimation and adaptation over Besov ellipsoids. *Bernoulli*, 26(3):1727–1764, 2020.
- Q. Chen, C. Xiang, M. Xue, B. Li, N. Borisov, D. Kaarfar, and H. Zhu. Differentially private data generative models. *arXiv preprint arXiv:1812.02274*, 2018.
- C. Cortes and V. Vapnik. Support-vector networks. *Machine learning*, 20(3):273–297, 1995.
- S. Dash, R. Dutta, I. Guyon, A. Pavao, K. P. Bennett, et al. Privacy preserving synthetic health data. In *ESANN 2019-European Symposium on Artificial Neural Networks, Computational Intelligence and Machine Learning*, 2019.
- T. L. Davis. *Teaching physiology through interactive simulation of hemodynamics*. PhD thesis, Massachusetts Institute of Technology, 1991.
- L. Dinh, J. Sohl-Dickstein, and S. Bengio. Density estimation using real NVP. *arXiv preprint arXiv:1605.08803*, 2016.
- J. Dong, A. Roth, and W. J. Su. Gaussian differential privacy. *arXiv preprint arXiv:1905.02383*, 2019.
- C. Dwork and G. N. Rothblum. Concentrated differential privacy. *arXiv:1603.01887v2*, 2016.
- C. Dwork, K. Kenthapadi, F. McSherry, I. Mironov, and M. Naor. Our data, ourselves: privacy via distributed noise generation. In *Advances in Cryptology: Proceedings of EUROCRYPT*, pages 485–503. Springer Berlin Heidelberg, 2006a.
- C. Dwork, K. Kenthapadi, F. McSherry, I. Mironov, and M. Naor. Our data, ourselves: Privacy via distributed noise generation. In *Annual International Conference on the Theory and Applications of Cryptographic Techniques*, pages 486–503. Springer, 2006b.
- C. Dwork, F. McSherry, K. Nissim, and A. Smith. Calibrating noise to sensitivity in private data analysis. In *Theory of cryptography conference*, pages 265–284. Springer, 2006c.
- C. Dwork, A. Smith, T. Steinke, and J. Ullman. Exposed! a survey of attacks on private data. *Annu. Rev. Stat. Appl.*, 4(1):61–84, 2017.
- E. B. Fowlkes and C. L. Mallows. A method for comparing two hierarchical clusterings. *Journal of the American statistical association*, 78(383):553–569, 1983.

- M. Germain, K. Gregor, I. Murray, and H. Larochelle. Made: Masked autoencoder for distribution estimation. In *International Conference on Machine Learning*, pages 881–889. PMLR, 2015.
- A. L. Goldberger, L. A. Amaral, L. Glass, J. M. Hausdorff, P. C. Ivanov, R. G. Mark, J. E. Mietus, G. B. Moody, C.-K. Peng, and H. E. Stanley. PhysioBank, PhysioToolkit, and PhysioNet: components of a new research resource for complex physiologic signals. *circulation*, 101(23):e215–e220, 2000.
- I. Goodfellow, J. Pouget-Abadie, M. Mirza, B. Xu, D. Warde-Farley, S. Ozair, A. Courville, and Y. Bengio. Generative adversarial nets. *Advances in neural information processing systems*, 27, 2014.
- E. P. Gordon, I. Schnittger, P. J. Fitzgerald, P. Williams, and R. L. Popp. Reproducibility of left ventricular volumes by two-dimensional echocardiography. *Journal of the American College of Cardiology*, 2(3):506–513, 1983.
- R. Hall, A. Rinaldo, and L. Wasserman. Differential privacy for functions and functional data. *The Journal of Machine Learning Research*, 14(1):703–727, 2013.
- K. K. Harrod, J. L. Rogers, J. A. Feinstein, A. L. Marsden, and D. E. Schiavazzi. Predictive modeling of secondary pulmonary hypertension in left ventricular diastolic dysfunction. *Frontiers in Physiology*, 12, 2021. URL <https://www.frontiersin.org/article/10.3389/fphys.2021.666915>.
- T. Heldt, R. Mukkamala, G. B. Moody, and R. G. Mark. CVSim: an open-source cardiovascular simulator for teaching and research. *The open pacing, electrophysiology & therapy journal*, 3: 45, 2010.
- N. Homer, S. Szelinger, M. Redmann, D. Duggan, W. Tembe, J. Muehling, J. Pearson, D. Stephan, S. Nelson, and D. Craig. Resolving individuals contributing trace amounts of dna to highly complex mixtures using high-density snp genotyping microarrays. *PLoS Genet*, 4:e1000167, 2008.
- S. Ioffe and C. Szegedy. Batch normalization: Accelerating deep network training by reducing internal covariate shift. In *International conference on machine learning*, pages 448–456. PMLR, 2015.
- J. Jälkö, O. Dikmen, and A. Honkela. Differentially private variational inference for non-conjugate models. *arXiv preprint arXiv:1610.08749*, 2016.
- J. Jälkö, L. Prediger, A. Honkela, and S. Kaski. Dpvm: Differentially private variational inference improved. *arXiv preprint arXiv:2210.15961*, 2022.
- A. Johnson, L. Bulgarelli, T. Pollard, S. Horng, L. A. Celi, and R. Mark. Mimic-IV. *PhysioNet*. Available online at: <https://physionet.org/content/mimiciv/1.0/> (accessed August 23, 2021), 2020.
- J. Jordon, J. Yoon, and M. Van Der Schaar. Pate-gan: Generating synthetic data with differential privacy guarantees. In *International conference on learning representations*, 2018.
- V. Karwa, D. Kifer, and A. B. Slavković. Private posterior distributions from variational approximations. *arXiv preprint arXiv:1511.07896*, 2015.
- D. P. Kingma and J. Ba. Adam: A method for stochastic optimization. *arXiv preprint arXiv:1412.6980*, 2014.

- D. P. Kingma and P. Dhariwal. Glow: Generative flow with invertible 1x1 convolutions. *Advances in neural information processing systems*, 31, 2018.
- D. P. Kingma and M. Welling. Auto-encoding variational Bayes. *arXiv preprint arXiv:1312.6114*, 2013.
- D. P. Kingma, T. Salimans, R. Jozefowicz, X. Chen, I. Sutskever, and M. Welling. Improved variational inference with inverse autoregressive flow. *Advances in neural information processing systems*, 29:4743–4751, 2016.
- M. Kroll. On density estimation at a fixed point under local differential privacy. *Electronic Journal of Statistics*, 15(1):1783–1813, 2021.
- N. Li, T. Li, and S. Venkatasubramanian. t-closeness: Privacy beyond k-anonymity and l-diversity. In *2007 IEEE 23rd international conference on data engineering*, pages 106–115. IEEE, 2007.
- F. Liu. Model-based differentially private data synthesis and statistical inference in multiply synthetic differentially private data. *Transactions on Data Privacy*, 15(3):141–175, 2022.
- A. Maceira, S. Prasad, M. Khan, and D. Pennell. Normalized left ventricular systolic and diastolic function by steady state free precession cardiovascular magnetic resonance. *Journal of Cardiovascular Magnetic Resonance*, 8(3):417–426, 2006.
- I. Mironov. Rényi differential privacy. In *2017 IEEE 30th Computer Security Foundations Symposium (CSF)*, pages 263–275. IEEE, 2017.
- A. Narayanan and V. Shmatikov. Robust de anonymization of large sparse datasets. *IEEE Symposium on Security and Privacy*, pages 111–125, 2008.
- G. Papamakarios, T. Pavlakou, and I. Murray. Masked autoregressive flow for density estimation. *Advances in neural information processing systems*, 30, 2017.
- N. Papernot, M. Abadi, U. Erlingsson, I. Goodfellow, and K. Talwar. Semi-supervised knowledge transfer for deep learning from private training data. *arXiv preprint arXiv:1610.05755*, 2016.
- N. Papernot, S. Song, I. Mironov, A. Raghunathan, K. Talwar, and Ú. Erlingsson. Scalable private learning with pate. *arXiv preprint arXiv:1802.08908*, 2018.
- M. Park, J. Foulds, K. Chaudhuri, and M. Welling. Variational Bayes in private settings (VIPS). *arXiv preprint arXiv:1611.00340*, 2016.
- B. Pfitzner and B. Arnrich. Dpd-fvae: Synthetic data generation using federated variational autoencoders with differentially-private decoder. *arXiv preprint arXiv:2211.11591*, 2022.
- T. J. Pollard, A. E. Johnson, J. D. Raffa, L. A. Celi, R. G. Mark, and O. Badawi. The eICU collaborative research database, a freely available multi-center database for critical care research. *Scientific data*, 5(1):1–13, 2018.
- D. Rankin, M. Black, R. Bond, J. Wallace, M. Mulvenna, G. Epelde, et al. Reliability of supervised machine learning using synthetic data in health care: Model to preserve privacy for data sharing. *JMIR Medical Informatics*, 8(7):e18910, 2020.
- D. Rezende and S. Mohamed. Variational inference with normalizing flows. In *International conference on machine learning*, pages 1530–1538. PMLR, 2015.

- D. B. Rubin. Statistical disclosure limitation. *Journal of official Statistics*, 9(2):461–468, 1993.
- P. Samarati and L. Sweeney. Protecting privacy when disclosing information: k-anonymity and its enforcement through generalization and suppression. *technical report, SRI International*, 1998.
- M. Sharma, M. Hutchinson, S. Swaroop, A. Honkela, and R. E. Turner. Differentially private federated variational inference. *arXiv preprint arXiv:1911.10563*, 2019.
- R. Shokri, M. Stronati, C. Song, and V. Shmatikov. Membership inference attacks against machine learning models. In *2017 IEEE symposium on security and privacy (SP)*, pages 3–18. IEEE, 2017.
- G. Simonneau, M. Gatzoulis, I. Adatia, C. Celermajer, D. and Denton, A. Ghofrani, M. Sanchez Gomez, R. Kumar, M. Landzberg, R. Machado, H. Olschewski, I. Robbins, and S. R. Updated clinical classification of pulmonary hypertension. *Journal of the American College of Cardiology*, 62(25 Supplement):D34–D41, 2013.
- L. Sweeney. Maintaining patient confidentiality when sharing medical data requires a symbiotic relationship between technology and policy. *Artificial Intelligence Laboratory, Massachusetts Institute of Technology*, AIWP-WP344, 1997.
- L. Sweeney. Matching Known Patients to Health Records in Washington State Data. *Social Science Research Network*, 2013. id=2289850.
- the SHARED team. The synthetic health and research data (shared) project, 2023. URL <https://shared.landenc.co/>. accessed on Jan 8, 2023.
- T. Tieleman, G. Hinton, et al. Lecture 6.5-rmsprop: Divide the gradient by a running average of its recent magnitude. *COURSERA: Neural networks for machine learning*, 4(2):26–31, 2012.
- S. Van Buuren and K. Groothuis-Oudshoorn. mice: Multivariate imputation by chained equations in R. *Journal of statistical software*, 45:1–67, 2011.
- C. Waites and R. Cummings. Differentially private normalizing flows for privacy-preserving density estimation. *arXiv preprint arXiv:2103.14068*, 2021.
- L. Wasserman and S. Zhou. A statistical framework for differential privacy. *Journal of the American Statistical Association*, 105(489):375–389, 2010.
- L. Xie, K. Lin, S. Wang, F. Wang, and J. Zhou. Differentially private generative adversarial network. *arXiv preprint arXiv:1802.06739*, 2018.
- A. Yale, S. Dash, R. Dutta, I. Guyon, A. Pavao, and K. P. Bennett. Generation and evaluation of privacy preserving synthetic health data. *Neurocomputing*, 416:244–255, 2020.
- K. Yared, P. Noseworthy, A. Weyman, E. McCabe, M. Picard, and A. Baggish. Pulmonary artery acceleration time provides an accurate estimate of systolic pulmonary arterial pressure during transthoracic echocardiography. *Journal of the American Society of Echocardiography*, 24(6):687–692, 2011.